Near Real-Time & Benchtop XRF Intercomparison for PM Elemental Analysis on Quartz and Teflon Filters: A Case Study Across Three European Cities

Stefanos Papagiannis[1,2], Manousos I. Manousakas[1], Dimitrios F. Anagnostopoulos[2], Michael Pikridas[3], Rima Baalbaki[3], Jean Sciare[3], Niall O'Sullivan[4], Stig Hellebust[4], John Wenger[4], Kirsten N. Fossum[5], Jurgita Ovadnevaite[5], Anja Tremper[6], David Green[6], Konstantinos Eleftheriadis[1], Evangelia Diapouli[1]

[1]ENvironmental Radioactivity & Aerosol Technology for atmospheric & Climate ImpacT Lab (ENRACT), Institute of Nuclear and Radiological Science & Technology, Energy & Safety (INRaSTES), NCSR Demokritos, Athens, 15341, Greece
[2]Department of Materials Science & Engineering, University of Ioannina, Ioannina, 45110, Greece
[3]Climate and Atmosphere Research Center, The Cyprus Institute, Nicosia, 2121, Cyprus
[4]School of Chemistry and Sustainability Institute, University College Cork, Cork, T12 K8AF, Ireland
[5]School of Natural Sciences, Ryan Institute's Centre for Climate & Air Pollution Studies, University of Galway, Galway, H91 TK33, Ireland
[6]MRC Centre for Environment and Health, Environmental Research Group, Imperial College London, London, W2 1PG, United Kingdom

Correspondence to: Stefanos Papagiannis (s.papagiannis@ipta.demokritos.gr), Evangelia Diapouli (ldiapouli@ipta.demokritos.gr)

Abstract. This study presents an extensive intercomparison between a benchtop X-ray fluorescence (XRF) system and near real-time XRF monitors (Xact 625 and 625i) for measuring elemental concentrations in ambient aerosols. The measurements were conducted across three locations: Athens (Greece, March 2024), Nicosia (Cyprus, March 2022–January 2023), and Dublin (Ireland, December 2022–February 2023). The primary focus was on comparing the performance of these near real-time and benchtop XRF systems for determining the elemental composition of particulate matter (PM), alongside evaluating the impact of filter substrate choice on measurement consistency. The study specifically examines the elements Si, S, Cl, K, Ca, V, Ti, Mn, Fe, Cu, Ni, Zn, Sr, and Pb. The results highlight that filter type plays a crucial role in ensuring accurate measurements when utilizing the benchtop XRF system. At the Athens site, where PTFE filters were used, the agreement between the Xact 625i and the benchtop XRF system was stronger, with slopes across the evaluated elements generally remaining closer to unity compared to the quartz substrates. In contrast, quartz fiber filters at the Dublin and Nicosia sites led to systematic deviations, especially for light elements such as S, Cl, and K, even after applying correction factors. For heavier elements like Fe, Mn, and Cu, the filter effect was less pronounced, though some variation across sites remained. Zn consistently showed good agreement, while Pb exhibited weaker correlation, possibly due to differences in the calibration curves of the two systems. Overall, this study not only evaluates instrument performance across multiple environments but also highlights how filter substrate selection impacts the comparability of these techniques, emphasizing the need for substrate-specific considerations to enhance consistency in elemental aerosol measurements.

1 Introduction

Particulate matter (PM) is a well-known major atmospheric pollutant, originating from both natural and anthropogenic sources, with significant impacts on health (Ostro et al., 2015; Samoli et al., 2013) and climate (Chen et al., 2021). Composed of a complex blend of chemical components, such as carbonaceous, ionic, and elemental species, the PM's composition varies widely depending on sources and environmental conditions, which contributes to its diverse chemical and physical characteristics.

The elemental analysis of atmospheric aerosols can offer information of critical value for health and source apportionment studies, which are vital for understanding pollution sources (Manousakas et al., 2021; Hopke et al., 2020), assessing population exposure risks (Megido et al., 2017; Caggiano et al., 2019), and implementing effective air quality management strategies. Exposure to certain elements, including As, Ni, Cr, Cd, and Pb, has been associated with an elevated cancer risk via inhalation (Aldekheel et al., 2023). These trace elements are also implicated in disrupting respiratory health by impairing mucociliary clearance, weakening barrier functions, inducing airway inflammation, promoting oxidative stress, and triggering cell apoptosis (Skalny et al., 2020).

Although elemental species do not substantially contribute to the overall mass of PM, they are crucial for accurately identifying pollution sources. The chemical signatures of the processes are mirrored in the emitted aerosol particles, enabling the use of specific elements to trace and allocate the sources of ambient aerosols effectively (Viana et al., 2008; Amato et al., 2016; Diapouli et al., 2017). For example, crustal elements like Al, Si, Ca and Fe serve as indicators of mineral dust (Viana et al., 2008; Jain et al., 2020); Cu and Zn are markers of brake and tire wear (Rhodes et al. 2012; Huang et al. 2018; Thorpe and Harrison 2008); and V and Ni may point to heavy oil combustion (Jang et al., 2007; Healy et al., 2009).

Consequently, the accurate assessment of the elemental composition of ambient aerosols is of vital importance. Traditionally, this elemental characterization has relied on laboratory-based, offline techniques such as Inductively Coupled Plasma Mass Spectrometry (ICP-MS), Particle Induced X-ray Emission (PIXE), and benchtop ED-XRF. While ICP-MS offers high sensitivity, it involves destructive and time-consuming sample preparation, whereas PIXE and benchtop ED-XRF provide non-destructive alternatives.

PM emissions and atmospheric dynamics, influenced by factors like wind direction and precipitation, can fluctuate within hours, affecting aerosol concentration and composition. Sampling on an hourly timescale (or at even higher time resolution) allows for a more detailed understanding of emission, transport, and deposition processes, enabling the capture of rapid source impacts. The recent advancements in high-time-resolution elemental analysis, especially by energy dispersive X-ray fluorescence (ED-XRF) spectrometers such as the Xact 625 and Xact 625i (SailBri Cooper, Inc.), the PX-375 (HORIBA, n.d.) and the ElvaX PmX-5050 (Elvatech, n.d), have significantly enhanced the ability to identify and trace pollution sources with greater time resolution (Manousakas et al., 2022; Rai et al., 2020). In addition, when equipped with an optional switching inlet system, those near real-time XRF spectrometers (NRT-XRF) also allow alternating automated sampling of both PM_{10} and $PM_{2.5}$ which greatly enhances the information regarding aerosol composition (Furger et al., 2020). However, a critical

difference between offline benchtop and online in-situ ED-XRF measurements is the trade-off between time resolution and mass loading. The higher temporal resolution of NRT-XRF inherently results in lower collected PM mass per sample. Consequently, online measurements must frequently contend with elemental concentrations that are much closer to the instrumental detection limits compared to traditional 24-hour offline samples.

A focused comparison of benchtop ED-XRF and NRT-XRF spectrometers, specifically regarding the measured elemental concentrations, is essential to determine their effectiveness in elemental monitoring of ambient aerosols. While past studies have evaluated the performance of NRT-XRF instruments, specifically the Xact 625 and 625i (Windell et al., 2025), these comparisons primarily involved ICP-MS (Furger et al., 2017; Tremper et al., 2018; Bhowmik et al., 2022) and, in only one case, the comparison of a benchtop ED-XRF spectrometer with an earlier Xact 625i model (Cadeo et al., 2025). This limited research underscores the need for a direct, updated comparison between current NRT and benchtop ED-XRF instruments to validate their performance in real-world conditions.

In addition to the need for direct instrument comparison, the choice of filter substrate significantly affects quantitative PM analysis in ED-XRF spectrometry (Unga et al., 2025). It is important to clarify that while NRT-XRF monitors like the Xact systems operate exclusively using continuous Teflon filter tape, offline sampling allows for different substrates to be selected prior to benchtop analysis. Consequently, the evaluation of filter choice in this study pertains specifically to the offline samples and how they compare against the standardized Teflon tape measurements of the Xact. Within many air quality monitoring networks, high-volume samplers routinely employ quartz fiber filters because of their compatibility with subsequent analyses of organic and ionic species. When extending these existing measurements to include elemental or metal characterization, it is often more practical to use the already collected quartz filters rather than perform additional co-located sampling on Teflon filters. However, this approach requires careful consideration of substrate-related effects when comparing these offline measurements to the NRT-XRF data. While many studies have examined Teflon and quartz fiber filter differences for organic and ionic species (Vecchi et al., 2009; Khuzestani et al., 2017; Aikawa and Hiraki 2010), there is limited literature regarding elemental characterization (Chiari et al., 2018; Yatkin et al., 2012). Chiari et al. (2018) emphasized the challenges when working with quartz fiber filters, which can introduce self-absorption and matrix effects due to their thickness, potentially leading to very high inaccuracies in concentration measurements, especially for lighter elements. Corrective methods are therefore essential when using quartz fiber filters to obtain accurate elemental concentrations.

For the reasons above, this study focuses on a detailed comparison between a benchtop ED-XRF and near real-time (NRT) XRF spectrometers (specifically the Xact 625 and 625i models) for measuring elemental concentrations in ambient aerosols, alongside an evaluation of filter substrate performance. Measurement campaigns were conducted in Athens, Greece (March 2024), Nicosia, Cyprus (March 2022–January 2023), and Dublin, Ireland (December 2022–February 2023), including quartz fiber and Teflon substrates for the comparison. Additionally, a dedicated filter substrate campaign was performed in January 2024. The results will compare the two instrument types across different environments and timeframes, providing insights into their consistency and applicability. Furthermore, the filter substrate comparison will assess the impact of Teflon

and quartz fiber filters on elemental quantification and offer practical recommendations for corrective procedures in aerosol studies.

2 Experimental

2.1 Sampling and Study area

Athens N.C.S.R. "Demokritos" station (ATH-DEM):

Measurements in Athens, specifically in Agia Paraskevi, were conducted at the urban background monitoring station located on the N.C.S.R. "Demokritos" campus (37°59'42.0"N, 23°48'57.6"E; 270 m above sea level) (Figure 1). This station is approximately 7 km northeast of central Athens and is situated at the base of Mount Hymettus. The station is part of the PANACEA National Infrastructure for Greece and provides representative data to the ACTRIS European infrastructure on urban background air quality due to its location, which is largely unaffected by direct emissions from urban PM sources (Zografou et al., 2022, Eleftheriadis et al., 2021).

A 24-hour sampling campaign took place from March 5 to March 25, 2024, resulting in 21 $PM_{2.5}$ samples. These samples were collected using Teflon filters (PTFE Pall R2PJ047 with PMP support ring, 47 mm diameter, 2 μm pore size) on a low-volume sampler (Sequential 47/50-CD, Sven Leckel GmbH, Berlin, Germany) operating at a flow rate of 2.3 m^3/h. Concurrently with the offline filter sampling, near real-time $PM_{2.5}$ elemental concentrations were measured continuously using an Xact 625i spectrometer. Over this same period (March 5 to March 25, 2024), the instrument collected a total of 498 hourly samples. In addition, an earlier campaign was conducted from January 13 to January 31, 2024, to investigate potential differences in elemental composition when using different filter substrates. This included 19 PM_{10} samples collected on Teflon filters (WHATMAN – PTFE, polypropylene-backed, pore size 1.0 μm, diameter 47 mm) and 19 PM_{10} samples collected on quartz fiber filters (PALLFLEX Tissue Quartz).

Cyprus Atmospheric Observatory (CAO-NIC):

Sampling was conducted at the Cyprus Atmospheric Observatory (CAO-NIC) urban background station of the Cyprus Institute premises in Nicosia (Athalassa Campus; 35°08'27.6"N 33°22'51.6"E; 174 m above sea level) (Figure 1). The site is located in a low-density residential area and is approximately 800 meters from the nearest major road and far from other significant anthropogenic sources. The Athalassa Forest Park lies to the southeast of the institute, further contributing to the minimal local pollution influences. Source apportionment studies (Bimenyimana et al., 2025; Bimenyimana et al., 2023; Christodoulou et al., 2023) show that PM at the site originates from a complex blend of local and regional sources. Regional air masses vary seasonally, bringing sulfate-rich air from Turkey and Eastern Europe in summer and dust mixed with anthropogenic pollutants from the Middle East and North Africa during other seasons. Local sources include biomass burning, traffic, power generation, and shipping activities.

$PM_{2.5}$ particles were collected on 47-mm diameter quartz filters (Tissuquartz 2500QUAT-UP, Pall) at 10 m above ground level (AGL) using a Leckel SEQ47/50 sampler operating at a flow rate of 2.3 m^3/h. After collection, the filters were placed in petri dishes and stored at -18 °C until further analysis. To ensure the proper functioning of the sampler, regular flow checks were performed throughout the campaign. A total of 256 filters were utilized over the course of the measurement period, from March 18, 2022, to January 17, 2023. Most samples were taken over 24-hour intervals, from 00:00 to 00:00 UTC. However, between December 16, 2022, to January 17, 2023, the sampling frequency was increased to every 8 hours corresponding to three collection periods: 02:00 – 10:00, 10:00 – 18:00, and 18:00 – 02:00. Alongside the offline filter collection, an Xact 625i spectrometer was deployed to monitor near real-time $PM_{2.5}$ elemental composition. During the full measurement period from March 18, 2022, to January 17, 2023, the Xact 625i successfully collected and analysed 6554 hourly samples.

Dublin Port Station (DUB-P):

Measurements were conducted in Dublin Port from 16 December 2022 to 7 February 2023 as part of the research project Source Apportionment of Air Pollution in the Dublin Port Area (PortAIR) (Fossum et al., 2025). Aerosol physicochemical properties and gaseous pollutants were measured using a suite of instrumentation housed in two containers. The monitoring site (53°20'54.4"N 6°11'40.8"W) (Figure 1) was selected to be downwind of most port activity and close to the ferries, which are a major daily source of shipping emissions (Fossum et al., 2024). A total of 54 $PM_{2.5}$ samples were collected onto quartz fiber filters (Pallflex, 150 mm diameter), pre-baked for 3 hours at 850°C, using a high-volume sampler (model DHA 80, Digitel) operating at a flow rate of 500 L min^{-1}. Following collection, the filters were individually packed and stored in a freezer at −18°C until analysis. In parallel with the high-volume sampling, near real-time $PM_{2.5}$ elemental measurements were conducted using an Xact 625 spectrometer. Throughout the campaign period (16 December 2022 to 7 February 2023), the instrument collected a total of 1887 hourly samples.

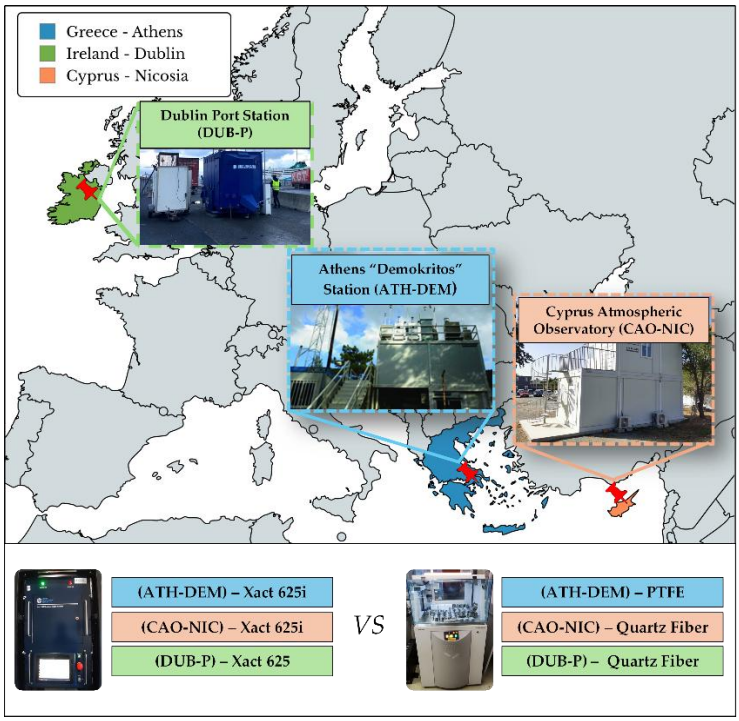

Figure 1: Locations of the measurement campaigns conducted in this study.

2.2 Instruments

2.2.1 Benchtop ED-XRF spectrometer

All offline $PM_{2.5}$ samples collected across the three measurement sites were analysed for major and trace elements using a single high-resolution energy-dispersive X-ray fluorescence (ED-XRF) spectrometer with advanced 3-D optics, the Epsilon 5 (PANalytical), located at the N.C.S.R. "Demokritos" campus in Athens, Greece. The spectrometer features a side-window, low-power X-ray tube equipped with a tungsten/scandium (W/Sc) anode. The characteristic X-ray radiation emitted by the samples is detected by a germanium (Ge) detector, offering an energy resolution of approximately 150 eV full-width at half-maximum (FWHM) at the Mn-Kα line (5.89 keV). To enhance measurement precision, the system employs six secondary targets (CaF_2, Ge, Mo, KBr, Al_2O_3, and LaB_6) that polarize the X-ray beam, allowing for six optimized measurement conditions tailored to the analysis of aerosol samples.

Calibration of the ED-XRF spectrometer was performed using a range of reference standards, including infinitely thin, single-element, compound, and multi-element materials. Specifically, 27 Micromatter thin-film standards deposited on 6.3 μm Mylar substrates were utilized, encompassing materials such as NaCl, MgF_2, GaP, SiO, KCl, CaF_2, V, Fe, Cr, Co, CuS_x, Al, Ni, CsBr, RbI, SrF_2, Ge, Se, Ag, Sn, Sb, Pt, AgHg, CdSe, Pb, Au, BaF_2, and Ce. Additionally, 22 multi-element standards were used, including one SRM 2783 standard and 21 UCDAVIS standards on polycarbonate and Teflon substrates. The reported uncertainty for Micromatter standards is 5%, while for multi-element standards, it is 10%. Each sample underwent

a 60-minute analysis. Prior to the final quantitative intercomparison, all reported ambient sample concentrations were blank-corrected by subtracting the average elemental concentrations measured on the corresponding field blank filters. The detection limits are calculated using the equation (Manousakas et al., 2018):

$$LoD = \frac{3\sqrt{Bkg}}{I\,t}\ \frac{1}{S} \quad (1)$$

here, LoD represents the detection limit in μg/cm², Bkg denotes the background counts of a field blank filter over a FWHM region centered at the element's principal peak centroid, I is the tube current in mA, t is the measurement time in seconds (s), and S refers to the sensitivity in $(\frac{counts}{s\,mA})/(\frac{\mu g}{cm^2})$. Figure 2a presents the detection limits for the measured elements on PTFE and quartz fiber blank filters in ng m^{-3}. However, because the quartz matrix (SiO_2) produces a massive intrinsic Si background, quantifying ambient aerosol Si on these substrates is unfeasible. Consequently, the mathematically calculated instrumental LoD for Si on quartz is considered physically meaningless in this context and has been excluded from all relevant figures and tables. To express the concentrations and detection limits in volumetric units (ng/m³), values in μg/cm² were first multiplied by the effective area of the filter (cm²) and then divided by the total sampled air volume (m³). This conversion accounts for the sampled air mass per unit volume and allows for direct comparison with ambient air quality standards.

The Quality Assurance/Quality Control (QA/QC) protocol for analysis includes a series of procedures to ensure high data quality and reliable instrument performance. The procedures involve: a) Weekly calibration of the Ge detector – The XRF software automatically fine-tunes the energy channels to maintain optimal detector performance; b) Regular performance evaluation using SRM 2783 – Weekly analyses of the multi-element reference material are conducted to verify analytical accuracy and precision for each analyte; c) Daily monitoring with PTFE blanks – Selected PTFE blank samples are systematically analysed to assess long-term reproducibility and ensure consistency across measurements. For daily instrument stability QA/QC checks, a specific PTFE filter was repeatedly measured to assess instrumental drift over time, providing a constant reference point to monitor instrument performance. Limits of detection for PTFE and Quartz fiber filters are presented in Table S1 in ng m^{-3}.

2.2.2 Near real-time (NRT) XRF spectrometers

The study utilized near real-time XRF spectrometers at three locations: Athens, Greece (ATH-DEM station, Xact 625i, Cooper Environmental Services (CES), Beaverton, OR, 129 USA), Dublin, Ireland (DUB-P station, Xact 625 Cooper Environmental Services (CES), Beaverton, OR, 129 USA), and Nicosia, Cyprus (CAO-NIC station, Xact 625i, Cooper Environmental Services (CES), Beaverton, OR, 129 USA). Both the Xact systems (625 and 625i) used in this study operate at a flow rate of 1 m³/h through a $PM_{2.5}$ cyclone, collecting particles on Teflon filter tape and analysing them hourly. Specifically, the systems utilize a step-and-measure operating sequence: after particulate matter is collected on a distinct spot of the tape for one hour, the tape advances. This moves the newly collected sample directly under the X-ray tube for analysis, while simultaneously, the next hourly sample begins collection on the fresh section of tape now positioned at the sampling inlet. During each analysis

cycle, the advanced sample is irradiated using a 50 kV, 50 W Rh-anode X-ray tube, and the resulting fluorescence is recorded by a silicon drift detector. Spectra are processed using the manufacturer's software to quantify elemental concentrations. The instruments run continuously, with simultaneous sampling and analysis, and routine QA checks (flow, calibration stability) are performed daily and at campaign start/end.

While sharing the same core analytical principles, the Xact 625 and Xact 625i represent different generations of the technology, leading to several operational and hardware differences. The Xact 625 is the earlier model, whereas the Xact 625i is an upgraded version with expanded capabilities. A primary difference lies in their analytical scope: the older Xact 625 deployed in Dublin (16 December 2022–7 February 2023) was configured to report up to 23 elements (Si–Pb), while the newer Xact 625i instruments (two distinct but identically configured units) in Athens (5–25 March 2024) and Nicosia (18 March 2022–17 January 2023) measured up to 35 elements (Al–Pb), reflecting the 625i's expanded hardware capability. Both 625i units operated with identical hardware settings and calibration protocols, ensuring no relevant analytical differences between the sites. Furthermore, the internal calibration standards differ between the two; the Xact 625 uses Palladium (Pd) as its internal calibration standard, whereas the Xact 625i uses Niobium (Nb).

The limits of detection for the Xact 625i and 625 are determined for each element using its sensitivity and the background counts from a blank, unused section of the tape. The reported values correspond to 1σ interference-free detection limits. For this study, a 60-minute time resolution was used. The limits of detection for Xact 625 and 625i are calculated using the equation (Rai, 2020):

$$LoD_{\sigma_0} = \frac{\sigma_0}{V} = \frac{\sqrt{Bkg\ t\ I}}{S\ t\ I}\ \frac{1}{V} \quad (2)$$

where, σ_0 represents the 68% confidence level detection limit, Bkg is the background count rate in $counts/(s\ \mu A)$, t is the live time in seconds (s), I is the current in μA, S is the sensitivity in $(\frac{counts}{s\ mA})/(\frac{\mu g}{cm^2})$ and V is the sample volume in m^3. Figure 2b presents the LoDs of the Xact 625 and Xact 625i spectrometers in ng/m³ (as reported by the manufacturer).

Quality assurance procedures for the Xact 625 and Xact 625i included daily energy calibration, response-stability checks for Cd, Cr, and Pb, and independent flow-rate verifications. Tape blanks were collected before and after filter-tape changes to ensure accuracy. Calibration with thin-film standards was performed when necessary to maintain measurement precision. The limits of detection for both instruments are presented in Table S2 (ng m^{-3}).

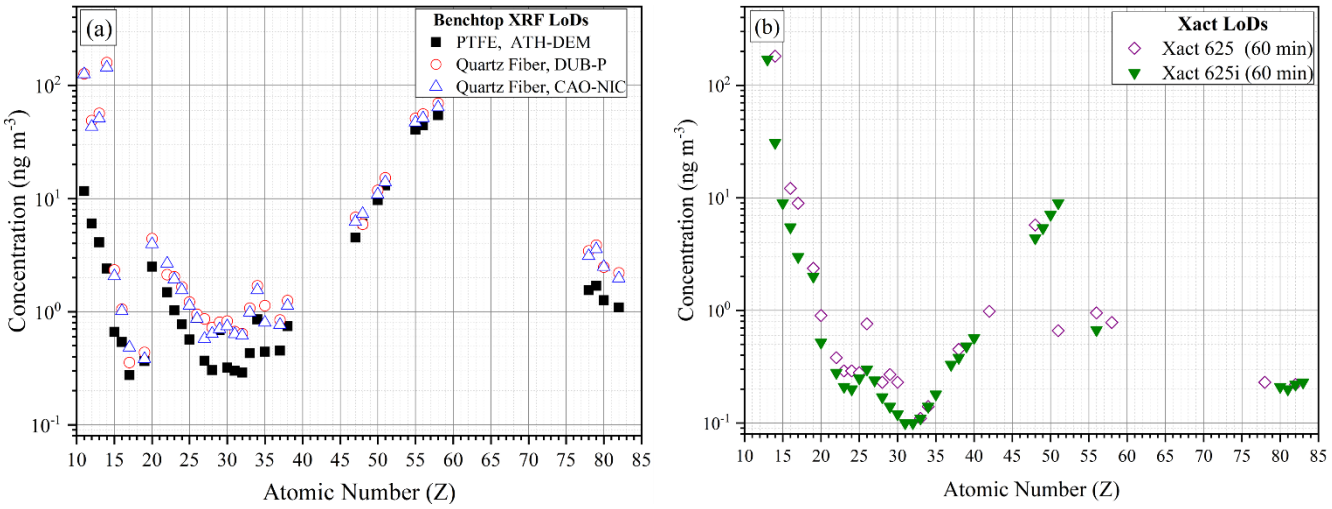

Figure 2: a) Limits of detections for the benchtop XRF spectrometer, for PTFE and Quartz fiber filters in ng m^{-3}. b) Limits of detections for the Xact 625 and 625i for 60-minute time resolution.

3 Results

3.1 Impact of PTFE and Quartz fiber filter substrates on aerosol elemental analysis with ED-XRF

In this study, benchtop ED-XRF measurements were performed on quartz fiber filters at the CAO-NIC and DUB-P sites. Because the characteristic X-ray signal response can depend on the filter matrix and thickness, it is essential to assess substrate-related effects prior to comparing data from the two systems. Evaluating the behaviour of PTFE versus quartz fiber filters therefore provides a necessary basis to ensure that observed differences between the benchtop XRF and the Xact originate from instrument performance and aerosol characteristics, rather than from substrate-induced analytical bias.

The comparison of ED-XRF measurements on PTFE and quartz fiber filters underscores the influence of aerosol penetration into the quartz matrix, particularly affecting low-energy X-rays (light elements). PTFE filters, with a typical thickness of 40–50 µm, retain particles on the surface and are thus considered "infinitely thin" for XRF analysis (Chiari et al., 2018). In contrast, quartz filters— with thickness approximately at 400–600 µm —act as bulk substrates, with particles depositing both on the surface and up to ~20 µm deep (Castaneda et al., 1998; Žitnik et al., 2008). Additionally, SEM analysis by Suárez-Peña et al. (2016) confirmed the isotropic structure of quartz fibers, showing non-uniform voids and deep particle penetration, especially for submicron aerosols. Particles <1 µm can reach depths beyond 300 µm, with those 0.1–0.5 µm accumulating in the inner layers (300–600 µm) due to Brownian diffusion, while larger particles are captured in the outer layers via interception and impaction.

When using quartz fiber filters, attenuation effects impact the measurement of light elements by weakening low-energy X-rays. Aerosol particles that penetrate the porous quartz matrix experience filter attenuation, as the emitted low-energy X-rays are absorbed by the thick filter material before escaping. Additionally, the substantial Si matrix from quartz fiber filters

not only hinders the precise measurement of lighter elements (Na, Mg, and Al) but also enhances the spectral background and peak overlaps. While these matrix effects and batch-to-batch filter variations pose analytical challenges, the required correction factors are often comparable to the slopes derived from empirical intercomparisons. Furthermore, several studies have successfully demonstrated that with opportune calibrations and correction protocols, ED-XRF can be reliably performed on quartz filters, even for light elements (Yatkin et al., 2012; Gupta et al., 2021; Dinoi et al., 2024; Potì et al., 2025; Unga et al., 2025). Regarding network standardization, the recent ACTRIS/GAW standard procedures for aerosol in-situ measurements (CAIS-ECAC: ACTRIS, 2024) suggest the use of thin PTFE or polycarbonate filters for XRF, reserving quartz fiber filters for inductively coupled plasma (ICP) measurements. It is important to note, however, that this is a suggestion for a standard operating procedure within a research network aimed at maximizing comparability, rather than an absolute methodological limitation.

To assess the impact of filter type on ED-XRF measurements, we compared elemental concentrations from 21 quartz fiber and 21 Teflon 24-hour PM_{10} filters (Section 2.1), evaluating differences due to particle penetration and X-ray attenuation. The selection of elements for this specific substrate analysis was strictly limited to those with ambient concentrations consistently exceeding the limit of quantification (LOQ) on both filter types during the campaign period. Elements falling below this threshold were excluded to ensure the reliability of the derived regression slopes. Since substrate-induced X-ray attenuation predominantly impacts low-energy X-rays, the elements meeting this mutual >LOQ criterion provided sufficient data to fully evaluate the attenuation effects for lighter elements, which was the primary objective of this dedicated comparison.

Although this comparison was performed on PM_{10} samples, it remains highly relevant to our $PM_{2.5}$ dataset, as the elements most affected by attenuation — S, Cl, K—are primarily associated with fine fraction aerosols. Gini et al. (2022) reported that fine elemental Sulfur, mainly present as sulfate (SO_4^{2-}), originates from anthropogenic sources and is predominantly found in the submicron range (0.1–1 μm). Similarly, potassium exhibits a bimodal distribution, while its coarse fraction is strongly influenced by local dust resuspension and Saharan dust transport—particularly in the Eastern Mediterranean—its fine fraction, linked to biomass burning, remains the dominant contributor to K in $PM_{2.5}$.

Linear regressions through the origin ($y = ax$) were performed to capture the proportional attenuation caused by the quartz filters, without introducing a baseline offset, because both filters were exposed to the same aerosol loading. Prior to forcing the linear regressions through the origin to derive the correction factors, standard unforced regressions were evaluated. The resulting intercepts were confirmed to be statistically compatible with zero ($p > 0.05$), justifying the use of a zero-intercept model. The comparison between PTFE and quartz fiber filters yielded strong correlations ($R^2 \geq 0.95$) across all analysed elements. Slopes represent the ratio of Teflon to quartz fiber concentrations, with values above unity indicating attenuation by the quartz filter. S exhibited the highest slope (1.87 ± 0.05), followed by Cl (1.51 ± 0.08) and K (1.48 ± 0.06), suggesting enhanced attenuation (Table 1). In contrast, elements such as Ca (1.00 ± 0.01), Fe (0.95 ± 0.08), showed slopes near unity, consistent with minimal filter-induced effects for heavier elements.

Table 1: Linear regression slopes and R^2 values for each element comparing Teflon and quartz fiber filters, from the measurement campaign (January 13 to January 31, 2024 - ATH-DEM station) to explore potential differences in elemental composition when using different filter substrates.

Element	Slope	R^2	Pair of Samples above LOQ
S	1.87 ± 0.05	0.98	17/19
Cl	1.51 ± 0.08	0.95	19/19
K	1.48 ± 0.06	0.97	19/19
Ca	1.00 ± 0.01	0.99	19/19
Ti	0.95 ± 0.02	0.99	10/19
Fe	0.95 ± 0.01	0.99	19/19
Ni	1.04 ± 0.04	0.95	8/19
Cu	0.98 ±0.02	0.99	11/19
Zn	1.07 ± 0.01	0.99	18/19

Based on these results, correction factors of 1.87, 1.51, and 1.48 were applied to S, Cl, and K measurements, respectively, while no corrections were applied to Ca, Ti, Fe, Ni, Cu, and Zn due to slopes close to unity and negligible substrate influence.

Additionally, from the recent study of Unga et al. (2025) on PM_{10} filters, it is shown that quartz fiber filters systematically yield lower concentrations for light elements such as S, Cl, and K compared to Teflon substrates (~0.6–0.7 C_{quartz}/C_{Teflon} ratios). Our results agree with this trend, as the Teflon/quartz fiber slopes obtained here for S (1.87), Cl (1.51), and K (1.48) (Table 1) correspond to inverse ratios of approximately 0.5–0.7, confirming similar attenuation effects in quartz fiber substrates for light elements. Figure 3 displays the comparison of elemental concentrations between Teflon and quartz fiber filters for S, K, Ca, and Fe.

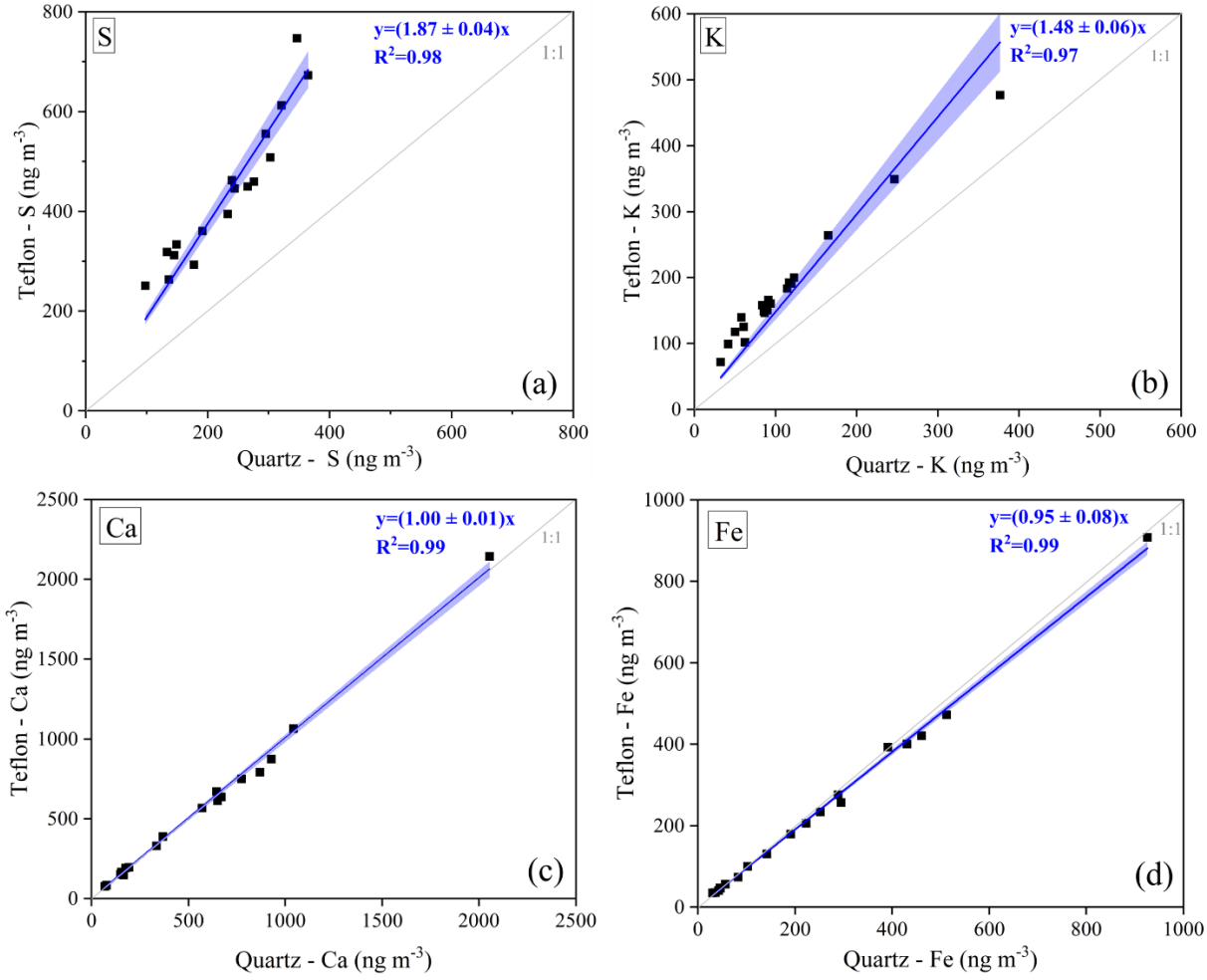

Figure 3: Comparison of Elemental Concentrations: Teflon vs. Quartz Filters of S (a), K (b), Ca (c) and Fe (d) using data from the dedicated measurement campaign conducted between January 13 and January 31, 2024, at the ATH-DEM station to explore potential differences in elemental composition across filter substrates. The shaded blue regions denote the 95% confidence intervals of the fitted regression slopes.

To further investigate attenuation effects, we simulated the characteristic intensities of S, Cl and K as a function of quartz fiber thickness utilizing the XMI-MSIM code (Schoonjans et al., 2013). The simulation incorporated the X-ray excitation energy (3.69 keV), spectrometer geometry, and detector characteristics of the Panalytical Epsilon 5 ED-XRF system. For quartz fiber thicknesses ranging from 1 to 450 µm, the normalized X-ray intensity showed a marked decrease due to absorption within the filter matrix. At 100 µm, the transmitted intensity dropped to approximately 0.30 for S, 0.36 for Cl, and 0.46 for K, confirming significant attenuation for lighter elements as the thickness of the quartz fiber filter increases (Figure 4). It is important to note that these simulated theoretical values were not utilized to derive the analytical correction factors applied to our dataset; rather, they serve as independent physical validation for the severe, element-specific attenuation behaviour observed in our empirical intercomparison.

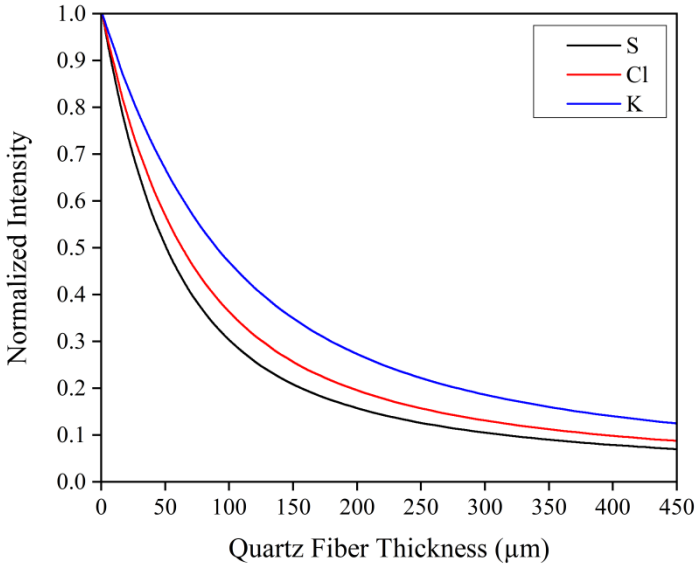

Figure 4: Normalized intensity of S, Cl and K as a function of quartz fiber thickness filter using the XMI-MSIM simulation code.

3.2 Comparative Analysis of NRT-XRF Monitors and Benchtop XRF Spectrometer: Data Processing

For the comparison between the NRT-XRF monitors (Xact 625 and Xact 625i) and the filter samples analysed by the benchtop XRF spectrometer, the hourly Xact measurements from corresponding days were averaged to match the 24-hour filter sample periods. Each 24-hour cycle included 23.5 hourly values from the Xact instruments, while the remaining half hour is utilized for the system's calibration check. For calculating the 24-hour average value, any hourly values reported below the LOD were substituted with LOD/2. Additionally, when quartz fiber filters were used, the measured concentrations of S, Cl, and K were multiplied by correction factors of 1.87, 1.51, and 1.48, respectively (Table 1).

For the quantitative analysis only values above the limit of quantification (LOQ) were used in the comparison, to ensure accuracy and reliability. The LOQ, defined as three times the limit of detection, represents the lowest concentration that can be quantified with acceptable precision and accuracy. Building on this, the following inclusion criterion was applied to select the final suite of elements evaluated for each site: an element was only included in the intercomparison analysis if its measured concentrations were consistently above the LOQ for both the benchtop ED-XRF and the respective Xact instrument. Consequently, the specific elements reported vary by measurement site depending on local atmospheric concentrations and the instrumental detection limits. If an element is reported for one site but excluded from another, it indicates that ambient concentrations at the excluded site fell predominantly below the detection capabilities of either the benchtop or the NRT-XRF system. This methodology directly explains why a larger number of elements are evaluated for the CAO-NIC station compared to ATH-DEM and DUB-P; the ambient aerosol mass loadings and elemental profile at CAO-NIC simply yielded a broader range of elements that successfully met this mutual >LOQ threshold. Furthermore, Aluminum (Al) was explicitly excluded

from all intercomparisons due to known hardware-related interferences in the NRT-XRF systems, which create an unstable background and limit reliable quantification for this specific element.

Linear regressions were performed using the model $y=ax+b$, as including an intercept allows detection of systematic offsets between instruments and avoids biasing the slope, consistent with best practice in instrument inter-comparison studies. In addition, 95% confidence intervals from the least-squares fit were included in the regression plots to illustrate the uncertainty in the relationship between the instruments.

To further assess the robustness and representativeness of the dataset, the number of samples with concentrations above the limit of quantification (>LOQ) relative to the total number of samples was evaluated for each site, instrument, and element (detailed in Table S3). For major elements such as sulfur (S), potassium (K), and iron (Fe), both the benchtop ED-XRF and the continuous Xact monitors achieved near 100% detection rates across all three campaigns, ensuring highly robust datasets for the subsequent regression analyses. Notably, for several trace metals, the Xact monitors successfully quantified a substantially higher number of samples >LOQ compared to the benchtop system. For instance, at the CAO-NIC site (out of 256 total pairs), the Xact 625i detected titanium (Ti) in 255 samples versus 128 for the benchtop, manganese (Mn) in 154 versus 66, and copper (Cu) in 146 versus 75. Similarly, at the DUB-P site (out of 50 total pairs), the Xact 625 quantified vanadium (V) in 46 samples compared to 23 for the benchtop, and nickel (Ni) in 49 compared to 30, highlighting the high sensitivity of the continuous monitors for these specific trace elements. Conversely, the benchtop ED-XRF demonstrated superior sensitivity for very light elements, as evidenced at the ATH-DEM site (out of 21 total pairs) where it successfully quantified silicon (Si) in all 21 samples, whereas the Xact 625i exceeded the LOQ in only 4 instances.

3.3 Benchtop XRF (PTFE) vs Xact 625i at the ATH-DEM station (March 5 - March 25, 2024)

Teflon filter samples analysed using the benchtop XRF system were compared with the corresponding Xact 625i measurements for eight elements (Si, S, Cl, K, Ca, Ti, Fe, and Zn). The linear regression slope and coefficient of determination (R^2) for each element are summarized in Table 2. Figure 5 presents the regression curves for Si, S, Fe, and Zn, while Figure 6 shows the time series graphs for S and Fe. Regression plots and time series for the remaining elements are provided in the Supplementary Information (SI).

Table 2: Summary of linear regression slopes and R^2 values for each element at the ATH-DEM, CAO-NIC, and DUB-P stations. The intercomparisons correspond to the benchtop ED-XRF offline filters versus the near real-time Xact monitors: ATH-DEM (Xact 625i vs. Teflon filters), CAO-NIC (Xact 625i vs. quartz fiber filters), and DUB-P (Xact 625 vs. quartz fiber filters).

	ATH-DEM station		CAO-NIC station		DUB-P station	
Element	**Slope**	**R^2**	**Slope**	**R^2**	**Slope**	**R^2**
Si	0.94 ± 0.19	0.88	–	–	–	–
S	0.97 ± 0.01	0.99	1.20 ± 0.07	0.49	1.58 ± 0.06	0.93
Cl	1.18 ± 0.09	0.95	3.10 ± 0.18	0.62	2.63 ± 0.13	0.89
K	0.66 ± 0.03	0.94	0.89 ± 0.02	0.83	0.78 ± 0.13	0.42
Ca	0.54 ± 0.04	0.88	1.72 ± 0.03	0.93	2.03 ± 0.30	0.66
Ti	0.72 ± 0.13	0.84	1.43 ± 0.03	0.94	–	–
V	–	–	–	–	1.37 ± 0.06	0.96
Mn	–	–	1.05 ± 0.06	0.81	–	–
Fe	0.66 ± 0.03	0.94	1.47 ± 0.03	0.91	1.63 ± 0.37	0.29
Ni	–	–	–	–	1.25 ± 0.12	0.78
Cu	–	–	0.67 ± 0.05	0.72	–	–
Zn	0.89 ± 0.10	0.77	1.02 ± 0.03	0.87	1.36 ± 0.13	0.81
Sr	–	–	0.63 ± 0.17	0.51	–	–
Pb	–	–	0.46 ± 0.14	0.15	–	–

Only four measurements for silicon (Si) were above the limit of quantification (LOQ) for the Xact 625i, reflecting the spectrometer's limited sensitivity for this element. This highlights one of the key limitations of the Xact 625i compared to the benchtop XRF system—its generally higher limits of detection (LoDs) in the lighter elements like Si, which can hinder accurate quantification, particularly for elements with low ambient concentrations. Nevertheless, for the Si data points above the LOQ, a slope of 0.94 ± 0.19 ($R^2 = 0.88$) was observed. While this slope is near unity, the very limited number of valid data points (n=4) precludes robust statistical conclusions; therefore, this result should be interpreted with caution as a preliminary observation of comparability rather than definitive agreement. In contrast, sulfur (S) exhibited excellent performance across both systems, with a slope of 0.97 ± 0.01 and an R^2 of 0.99, demonstrating a near-perfect correlation and underscoring the Xact 625i's robustness in measuring this element. Chlorine (Cl) demonstrated a slope of 1.18 ± 0.09 ($R^2 = 0.95$), indicating a strong correlation with a slight deviation from unity. Potassium (K) showed a slope of 0.66 ± 0.03 ($R^2 = 0.94$), suggesting consistent trends despite a systematic difference in concentrations. Calcium (Ca) and titanium (Ti) exhibited slopes of 0.54 ± 0.04 ($R^2 = 0.88$) and 0.72 ± 0.13 ($R^2 = 0.84$), respectively. Iron (Fe) displayed a slope of 0.66 ± 0.03 ($R^2 = 0.94$), indicating a strong linear correlation, though the slope well below unity reflects a systematic difference, with the Xact 625i reporting lower concentrations relative to the benchtop system. Although the slopes below unity suggest systematic underestimation by the Xact 625i for some elements, the consistently high R^2 values confirm reliable and reproducible trends across both systems.

Zinc (Zn), with a slope of 0.89 ± 0.10 ($R^2 = 0.77$), showed moderate correlation, where the slope near unity reflected comparable measurements, while the lower R^2 indicated greater variability.

The average slope of 0.82 and average R^2 of 0.91 indicated a strong overall correlation between the benchtop XRF spectrometer and the Xact 625i, suggesting that both instruments produced consistent measurements across the elements evaluated in this study. The slope slightly below 1 implied a systematic difference in quantification, where the Xact 625i tended to report lower values compared to the benchtop XRF.

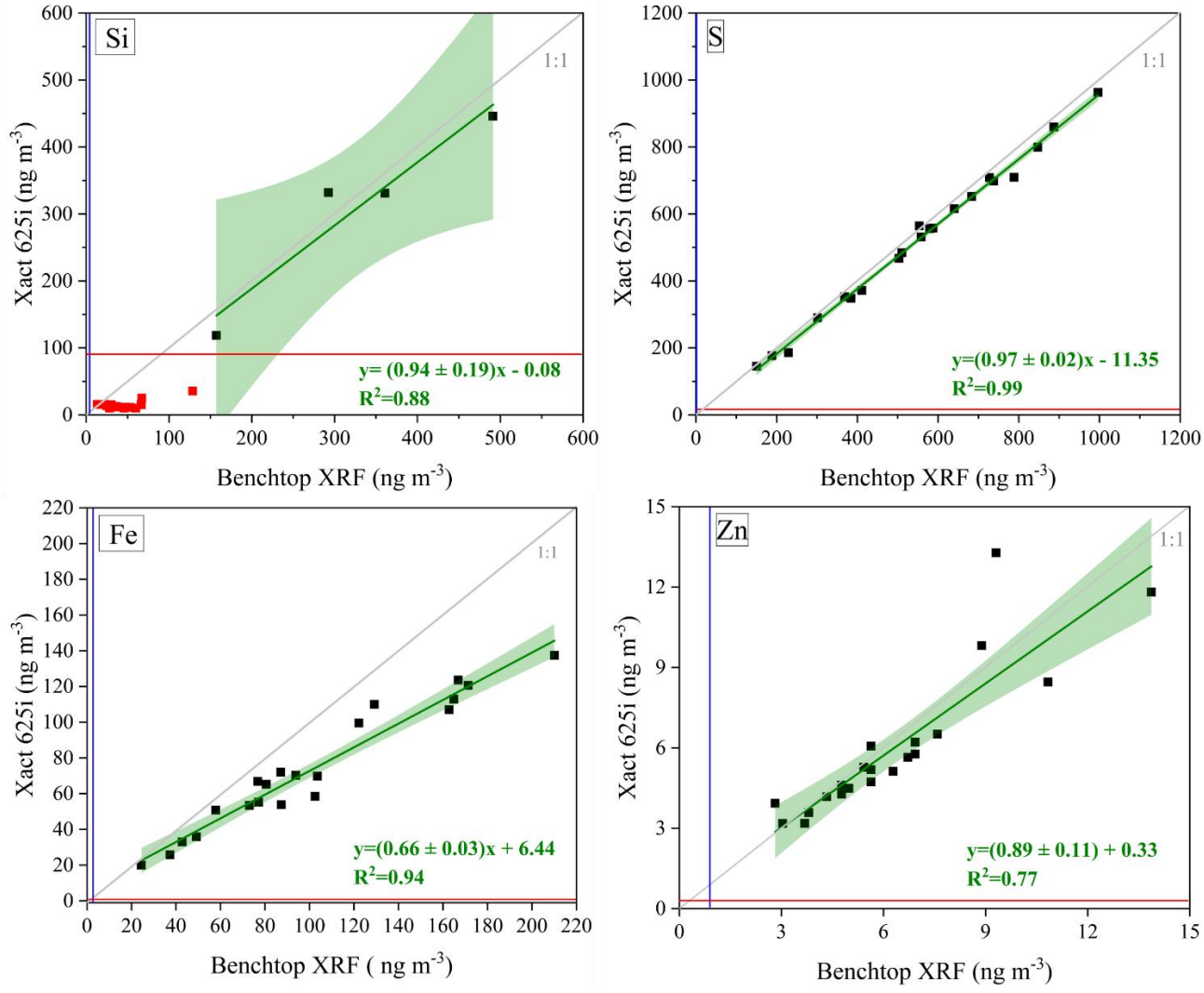

Figure 5: Comparison of elemental concentrations in ng m^{-3} for Si, S, Fe, and Zn for the ATH-DEM station. The blue lines indicate the LOQ threshold for the benchtop XRF spectrometer, while the red lines represent the corresponding threshold for the Xact 625i continuous elemental monitor. The grey line represents the 1:1 reference line, while the green line represents the linear regression fit. Data points below the LOQ were excluded from the analysis to ensure accurate comparison between the two instruments and are highlighted in red, distinguishing measurements with higher uncertainty.

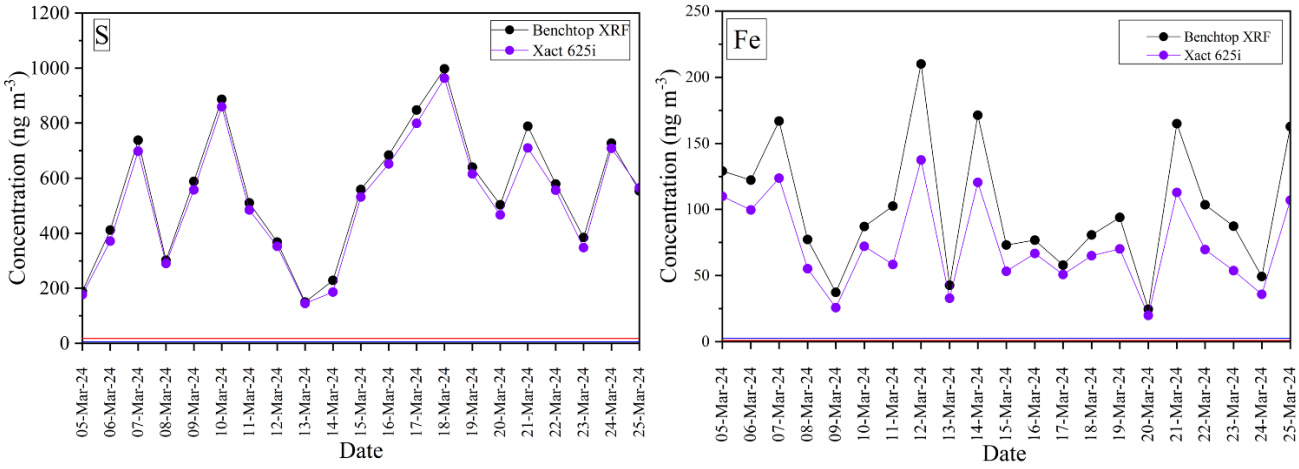

Figure 6: Time series graphs comparing S and Fe concentrations (ng m⁻³) from March 5 to 25, 2024, show strong agreement for S, while Fe exhibits a consistent deviation, with lower values reported by the Xact 625i. This suggests differences in the calibration curves for heavier elements between the instruments. The red and blue lines indicate the LOQ thresholds for the Xact 625i and the benchtop XRF spectrometer, respectively.

3.4 Benchtop XRF (Quartz Fiber) vs Xact 625i at the CAO-NIC Station (March 18, 2022 – January 17, 2023)

At the CAO-NIC site, benchtop XRF measurements were performed on quartz fiber filters. Table 2 presents the linear regression slopes and R^2 values for each element, compared with the corresponding Xact 625i measurements. Figure 7 presents the regression curves for S, Cl, K and Zn, while Figure 8 shows the time series graphs comparing K and Zn. Regression plots and time series for the remaining elements are provided in Supplementary Information (SI).

Sulfur (S) exhibited a slope of 1.20 ± 0.15 (R^2 = 0.49), reflecting moderate agreement between the instruments and some remaining variability after correction. Chlorine (Cl) presented a slope of 3.10 ± 0.18 (R^2 = 0.62), indicating a moderate relationship with higher variability relative to unity, which may relate to particle penetration and absorption within the quartz matrix as well as potential chloride volatility (e.g., ammonium chloride loss). Potassium (K) showed a slope of 0.89 ± 0.07 (R^2 = 0.83), demonstrating good agreement between systems. While the applied correction factors improved the comparability for elements like K, significant discrepancies remain evident, particularly for S and Cl. These pronounced residual differences are likely linked to the heterogeneous structure and variable porosity of quartz fiber filters, which can influence attenuation differently between batches, along with instrument-specific and site-dependent aerosol characteristics. Thus, rather than minor deviations, the remaining variability highlights the persistent limitations of quartz substrates. While the empirical corrections mitigate the most severe attenuation effects, achieving high consistency and reliability across the two platforms for the lightest and most sensitive elements remains highly challenging.

Calcium (Ca) and titanium (Ti) displayed slopes of 1.72 ± 0.03 (R^2 = 0.93) and 1.43 ± 0.03 (R^2 = 0.94), respectively, both showing high correlation and comparable measurements. Manganese (Mn) had a slope of 1.05 ± 0.06 (R^2 = 0.81), indicating strong agreement. Iron (Fe) exhibited a slope of 1.47 ± 0.03 (R^2 = 0.91), reflecting a consistent trend between

instruments. Copper (Cu) had a slope of 0.67 ± 0.05 (R^2 = 0.72), suggesting a moderate correlation with some variability. Zinc (Zn) presented a slope of 1.02 ± 0.03 (R^2 = 0.87), indicating highly comparable measurements. Strontium (Sr) exhibited a slope of 0.63 ± 0.17 (R^2 = 0.51), indicating moderate agreement with some residual variability, while lead (Pb) remained lower at 0.46 ± 0.14 (R^2 = 0.15), reflecting weaker correlation and higher measurement uncertainty.

In addition to the overall agreement, several distinct events were observed where elemental concentrations peaked simultaneously in both the Xact 625i and the benchtop XRF measurements, particularly for calcium (Ca), titanium (Ti), iron (Fe) and manganese (Mn). During these events, the time series from both instruments showed consistent patterns, indicating that they captured the same atmospheric variability. However, the Xact 625i consistently reported higher concentrations, which is likely attributable to differences in the calibration procedures between the two instruments.

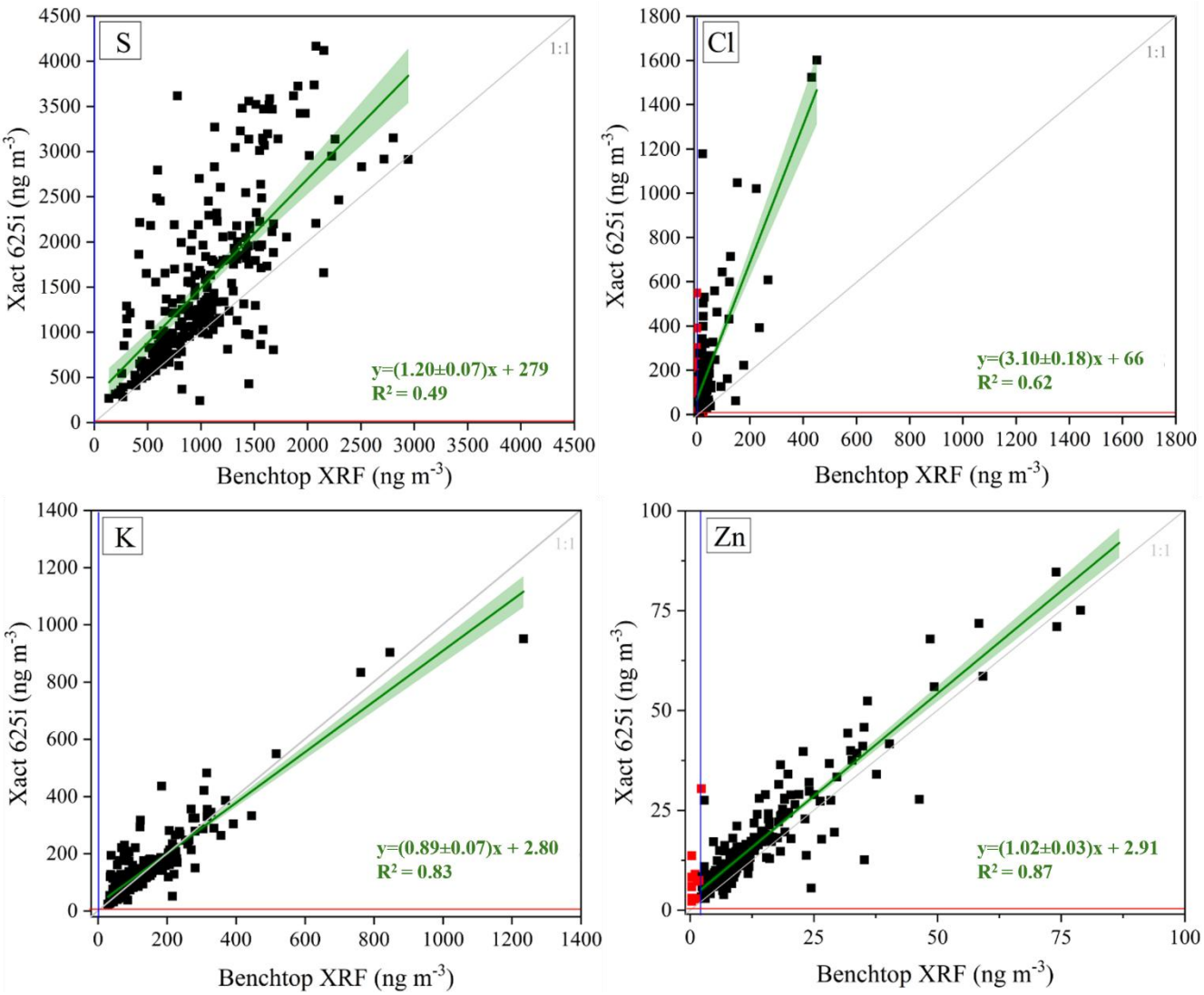

Figure 7: Comparison of elemental concentrations in ng m^{-3} for S, Cl, K and Zn for the CAO-NIC station. The blue lines indicate the LOQ thresholds for the benchtop XRF spectrometer, while the red lines represent the corresponding thresholds for the Xact 625i continuous elemental monitor. The grey line represents the 1:1 reference line, while the green line represents the linear regression fit. Data points below the LOQ were excluded from the analysis to ensure accurate comparison between the two instruments and are highlighted in red, distinguishing measurements with higher uncertainty.

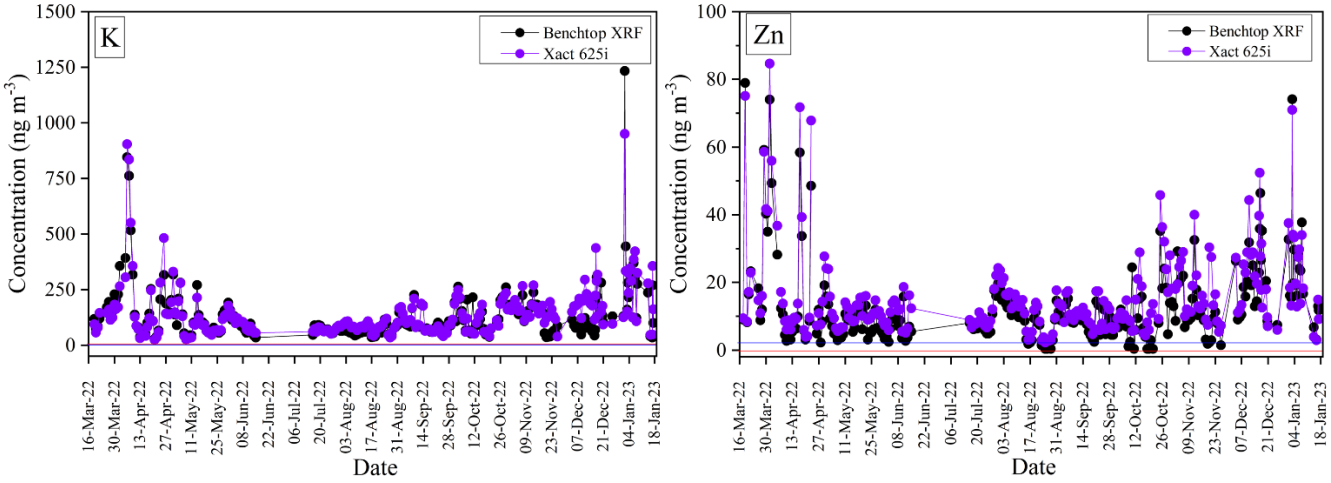

Figure 8: Time series graphs comparing K and Zn concentrations in ng m^{-3} from 16 March 2022 to 18 January 2023. The red and blue lines indicate the LOQ thresholds for the Xact 625i and the benchtop XRF spectrometer, respectively.

3.5 Benchtop XRF (Quartz Fiber) vs Xact 625 at the DUB-P Station (December 16, 2022 – February 7, 2023)

Figure 9 presents the regression curves for the elements S, Cl, V, and Ni, while Figure 10 shows the time series graphs for Cl and Zn. Regression plots and time series for the remaining elements are provided in the Supplementary Information (SI). Benchtop XRF measurements were performed on quartz fiber filters collected at the DUB-P site. Sulfur (S) displayed a slope of 1.58 ± 0.06 (R^2 = 0.93), indicating strong agreement between the instruments. Chlorine (Cl) showed the highest slope at 2.63 ± 0.13 (R^2 = 0.89), suggesting a systematic difference while maintaining a strong correlation. Potassium (K) had a slope of 0.78 ± 0.13 (R^2 = 0.42), reflecting a weaker correlation and more variability in the measurements. Furthermore, as observed in the time series (Figure S4), K exhibits a clear systematic bias where the Xact 625 consistently reports higher concentrations than the benchtop XRF. Calcium (Ca) demonstrated a slope of 2.03 ± 0.30 (R^2 = 0.66), indicating a notable deviation from unity with moderate agreement. Vanadium (V) exhibited a slope of 1.37 ± 0.06 (R^2 = 0.96), reflecting a strong linear correlation, though the slope indicates a systematic difference in quantification between the two instruments. Iron (Fe) showed a slope of 1.63 ± 0.37 (R^2 = 0.29), indicating substantial variability and a weaker relationship. The lower correlation coefficients and greater variability observed for these specific elements (Fe, Ca, and K)—especially when compared to the stronger alignments seen at the ATH-DEM and CAO-NIC stations—are largely attributable to systematic differences in the calibration curves between the older Xact 625 model used at this site and the benchtop XRF system. Nickel (Ni) had a slope of 1.25 ± 0.12 (R^2 = 0.78), representing reasonable agreement with some deviation. Zinc (Zn) displayed a slope of 1.36 ± 0.13 (R^2 = 0.81), showing a strong correlation between the two instruments. Table 2 presents the linear regression slopes and R^2 values for each element at the DUB-P station.

The average slope of 1.6 and average R^2 of 0.7 for the DUB-P campaign indicated a moderate overall agreement between the benchtop XRF spectrometer and the Xact 625. Although the correlation varies across elements, the results

highlight consistent trends for most elements, with stronger agreement for sulfur (S), vanadium (V), and zinc (Zn), while potassium (K) and iron (Fe) exhibited greater variability.

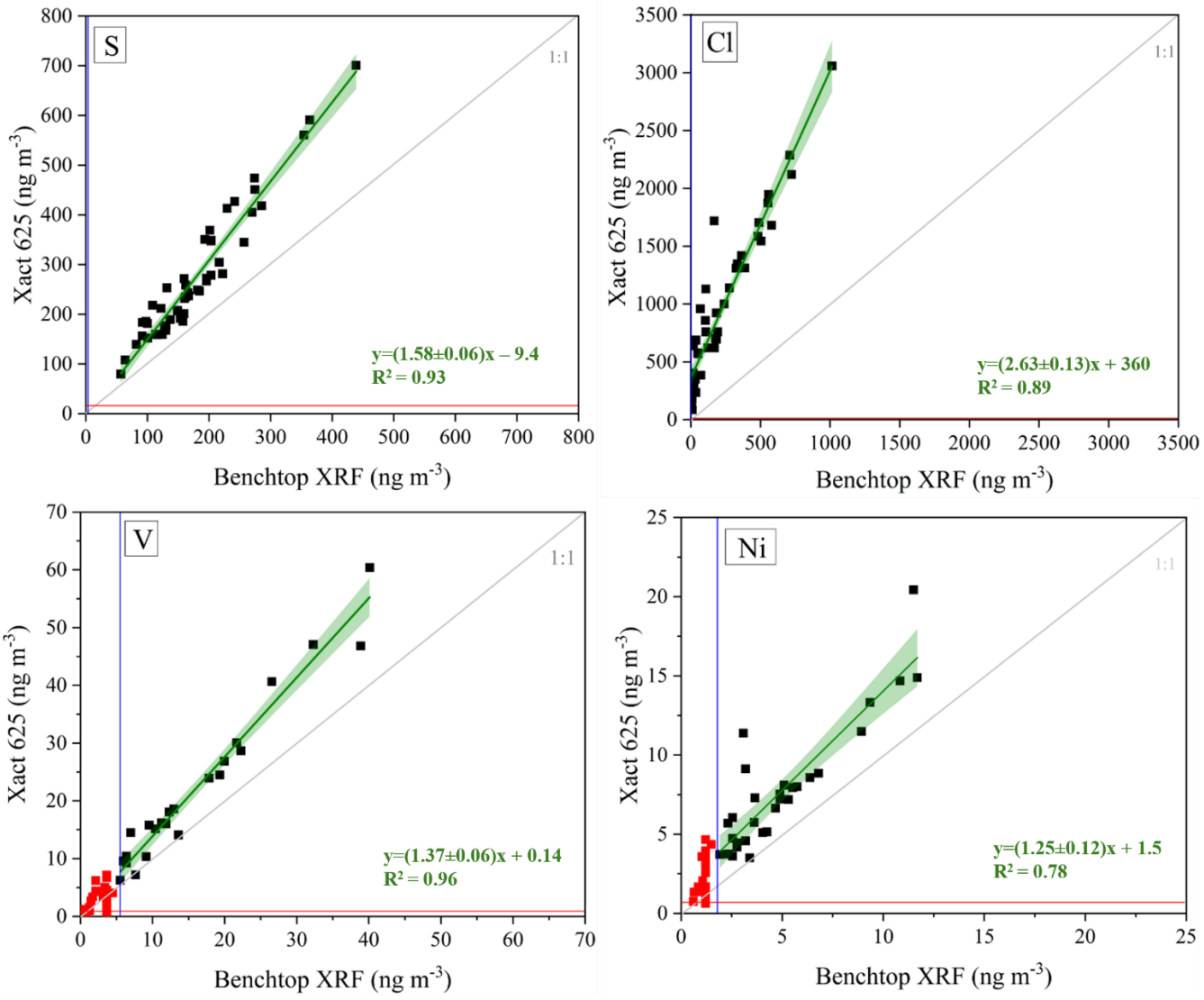

Figure 9: Comparison of elemental concentrations in ng m^{-3} for S, Cl, V and Ni for the DUB-P station. The blue lines indicate the LOQ thresholds for the benchtop XRF spectrometer, while the red lines represent the corresponding thresholds for the Xact 625 continuous elemental monitor. The grey line represents the 1:1 reference line, while the green line represents the linear regression fit. Data points below the LOQ were excluded from the analysis to ensure accurate comparison between the two instruments and are highlighted in red, distinguishing measurements with higher uncertainty.

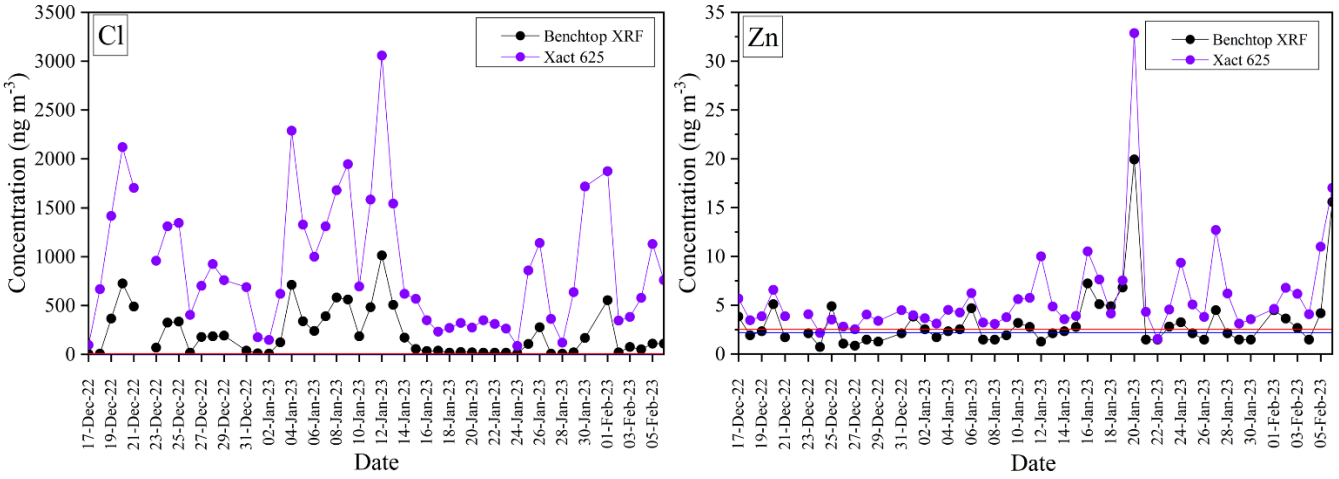

Figure 10: Time series graphs comparing Cl and Zn concentrations (ng m^{-3}) at the Dub-P station, show a systematic difference, with the benchtop XRF consistently reporting lower concentrations than the Xact 625. This suggests that the quartz fiber filter may introduce systematic deviations, particularly for light elements, while differences in calibration curves between the instruments could also play a role. The red and blue lines indicate the LOQ thresholds for the Xact 625 and the benchtop XRF spectrometer, respectively.

4 Discussion

The effect of filter type on measurement consistency is evident across the three sites. At ATH-DEM (PTFE filters) the comparison between the Xact 625i and the benchtop XRF spectrometer shows slopes consistently closer to unity for most elements. The consistently high R^2 values (R^2 = 0.77 – 0.99) across most elements suggest minimal variability, meaning the continuous XRF monitors provides results comparable to those from the benchtop XRF. However, it has to be noted that while the agreement for Si is encouraging, it also highlights the generally higher limits of detection (LoDs) of the Xact 625i for lighter elements (K and below), which can limit its sensitivity in low-concentration environments. Other elements, such as chlorine (Cl), iron (Fe), and potassium (K), also show high R^2 values (R^2 = 0.94 – 0.95) despite deviations in slope, suggesting systematic differences rather than random variability. These systematic deviations are likely due to differences in instrument calibration, as each system may utilize distinct reference standards. Overall, the better alignment at ATH-DEM is likely aided by the lower X-ray attenuation associated with PTFE filters. Cadeo et al., (2025) recently reported strong agreement between the Xact 625i and benchtop XRF using mixed cellulose ester membrane filters (MCE) in Milan, with R^2 values up to 0.99 and slopes generally near unity for most elements, particularly metals. Similarly, our Athens comparison using PTFE filters showed high consistency across eight elements (average slope = 0.82, average R^2 = 0.91), with S and Si near unity and K, Ca, Ti and Fe showing slopes below one but strong correlations (R^2 = 0.84 – 0.94). The smaller subset of elements reported in our ATH-DEM campaign, compared to the Milan study, simply reflects the differing local ambient atmospheric concentrations, as additional elements at our site predominantly remained below the mutual quantification thresholds of the instruments. Both studies therefore confirm that the intercomparison between the Xact 625i and benchtop XRF is highly robust when thin, low-

attenuation filters (such as PTFE or MCE) are used for offline sampling, confirming the continuous monitor's ability to provide reliable elemental time-series information.

Despite the application of correction factors, the quartz fiber filter sites (DUB-P and CAO-NIC) continue to exhibit systematic deviations, particularly for lighter elements such as S, Cl, and K. Notably, S shows substantial higher concentrations at DUB-P, with a corrected slope of 1.58 ± 0.06, compared to a closer-to-unity value of 1.20 ± 0.07 at CAO-NIC. This difference is notable, especially considering the strong correlation at DUB-P ($R^2 = 0.93$), which implies consistent tracking of variability but a persistent offset in absolute values. One possible explanation for this discrepancy lies in the instrumental differences between the two sites: DUB-P employed the Xact 625, while CAO-NIC used the newer Xact 625i. This suggests a potential improvement in calibration or measurement accuracy in the upgraded version. Additionally, iron (Fe) shows poorer agreement at DUB-P, whereas elements like vanadium (V), nickel (Ni), and zinc (Zn) display relatively better performance. This contrast may reflect slight calibration mismatches or performance limitations specific to the older Xact 625 model. Furthermore, as established in Section 3.1, these instrumental differences are severely exacerbated by the inherent physical properties of the quartz fiber filters. Unlike thin PTFE, quartz filters are thick, non-uniform substrates that allow for variable and deep aerosol penetration into the matrix. This structural complexity generates a high spectral background that can vary significantly from one filter to the next. Even with rigorous field and laboratory blank subtraction, this inherent filter-to-filter spectral and physical variability introduces residual uncertainty that disproportionately may impact the quantification of elements.

At the CAO-NIC site, the comparison with the Xact 625i reveals both strong correlations and systematic differences across elements. Several elements, including Ca, Ti, Fe, Mn, and zinc (Zn), exhibit high R^2 values ($R^2 = 0.81 – 0.94$) and slopes near unity, indicating good agreement between the continuous and benchtop XRF systems. In contrast, chlorine (Cl) shows an elevated slope of 3.10 ± 0.18 ($R^2 = 0.70$), continuing the pattern seen at DUB-P, where the slope is 2.63 ± 0.13 ($R^2 = 0.89$). Cl is the most noteworthy element, with substantial deviations in slope at both sites, even after the application of correction factors. Despite efforts to account for the attenuation effects, the difference in slope for Cl is far more significant than for other light elements. This suggests that there may be an underlying issue with the Cl measurement itself, which may be attributed to the volatility of the element. Additionally, peak events in elemental concentrations—particularly for Ca, Ti, Fe, and Mn—were observed in both instruments, confirming their ability to track atmospheric variability. However, the Xact 625i systematically reported higher concentrations, further supporting the role of calibration differences. Despite those differences, the overall strong average R^2 of 0.62 and the robust agreement for many mid-to-heavy elements underscore the utility of the Xact 625i, while reinforcing the need for caution when interpreting light elements on quartz filters.

Overall, the filter type significantly influences measurement consistency. PTFE filters, as used at ATH-DEM, result in stronger agreement and more stable measurements across most elements. Quartz fiber filters, used at DUB-P and CAO-NIC, exhibit greater variability for light elements; however, correction efforts mitigate these effects and improve overall comparability, especially for S and K. Figure 11 presents the comparative concentration plots for the elements S, Cl, K, Ca, Ti, Fe and Zn between the continuous and benchtop XRF systems.

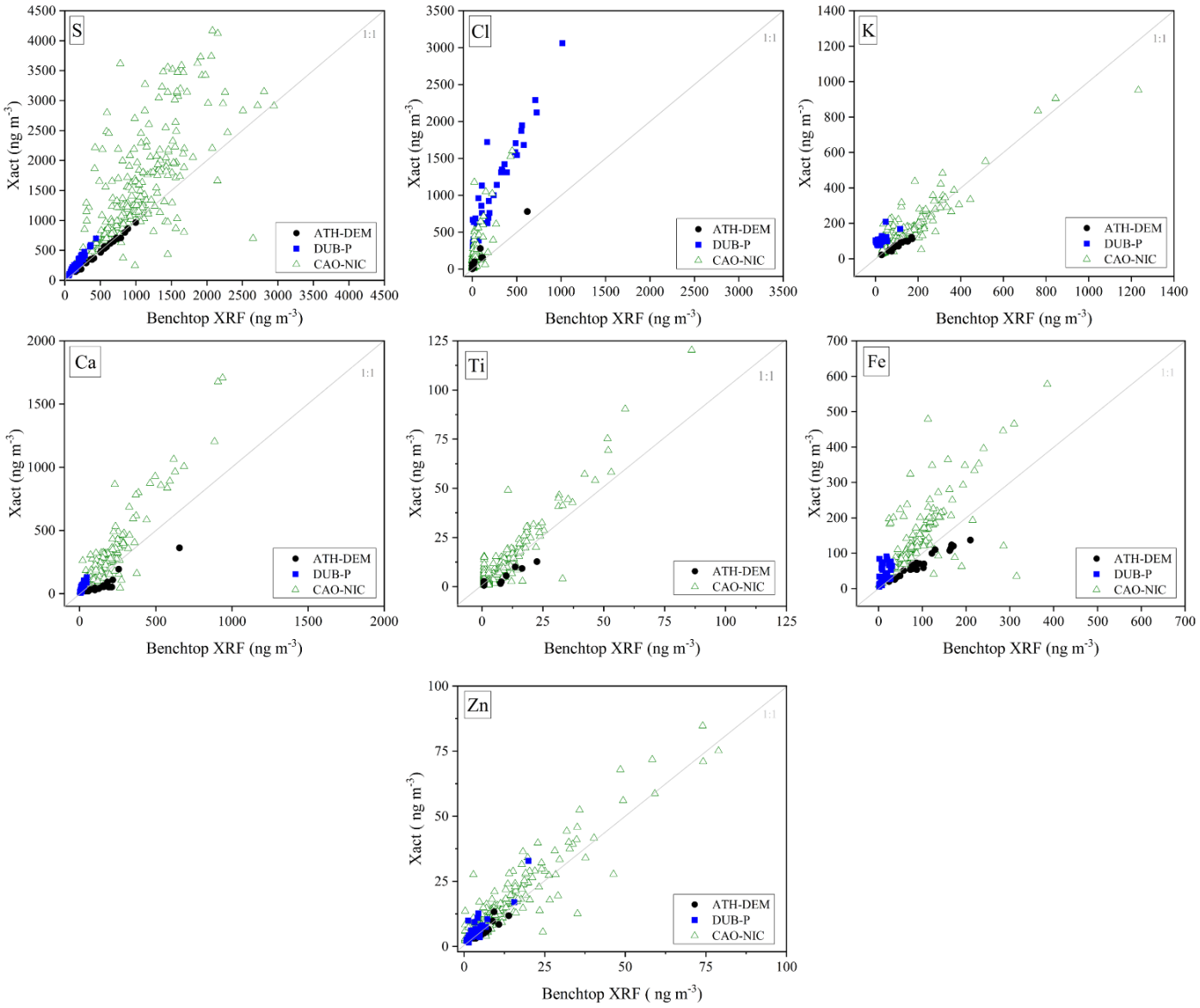

Figure 11: Comparison of elemental concentrations of S, Cl, K, Ca, Ti (Ti was not detected in DUB-P), Fe, Zn in ng m^{-3} for all stations.

5 Conclusions

This study conducted an extensive intercomparison between a benchtop ED-XRF and NRT-XRF spectrometers (Xact 625 and 625i) to evaluate their performance in measuring elemental concentrations in ambient aerosols across three locations: Athens (Greece), Dublin (Ireland), and Nicosia (Cyprus). A key focus was the influence of filter substrate of measurement results.

The findings highlight that filter type plays a critical role in the quantification of light elements. At the Athens site, where PTFE filters were used, the agreement between instruments was stronger, with slopes closer to unity and high R^2 values, indicating stable and consistent performance. In contrast, at the Dublin and Nicosia sites, which used quartz fiber filters, deviations were observed for sulfur (S), chlorine (Cl), and potassium (K) due to X-ray attenuation in the quartz matrix. Applying correction factors substantially improved agreement for S and K, demonstrating their effectiveness in mitigating substrate-related effects. For Cl, however, a residual positive bias remained likely influenced by both quartz interactions and chloride volatility. In addition, variability in quartz fiber filter composition, porosity, and thickness across filter batches may introduce inconsistent attenuation behaviour, complicating the application of a universal correction factor. Overall, while corrections enhanced comparability, quartz substrates still present challenges for light-element quantification. For heavier elements such as iron (Fe), manganese (Mn), and copper (Cu), the impact of filter type was less pronounced, but variations were still present across sites. Zinc (Zn) maintained good agreement across all locations, whereas lead (Pb) exhibited weaker correlation, suggesting additional influencing factors beyond filter type. Differences in the use of different calibration standards of the two instruments may have contributed to these discrepancies.

Overall, this study underscores the complexity of intercomparisons between different XRF instrument types and filter substrates, particularly for light elements. Quartz fiber filters, in particular, introduce greater variability due to enhanced X-ray attenuation. Therefore, when using quartz fiber filters in ambient aerosol studies, it is essential to implement element-specific correction protocols and consider substrate-related uncertainties during data interpretation. For more reliable and consistent measurements, especially of light elements, PTFE filters are recommended. Additionally, harmonization of calibration procedures across instruments may help reduce discrepancies. These findings highlight the importance of carefully selecting both instrumentation and filter media in XRF-based aerosol analysis to ensure data comparability across monitoring networks. Ultimately, this study confirms that near real-time XRF monitors (like the Xact 625i) are highly reliable, state-of-the-art instruments capable of capturing high-resolution temporal dynamics. However, they are not designed to replace traditional filter-based benchtop systems. While NRT monitors can technically be adapted to analyze offline filters for a limited number of measurements, routine operation in this manner is extremely time-consuming and practically unfeasible. The two instrument categories address fundamentally different analytical needs; offline analysis remains indispensable for high-throughput sample processing, physical sample archiving, and multi-technique chemical characterization. Therefore, working in tandem with NRT systems—rather than viewing one as a substitute for the other—allows for a highly comprehensive and robust understanding of ambient aerosol elemental composition.

Data availability. The dataset containing the near real-time $PM_{2.5}$ elemental concentrations measured by the Xact spectrometer at the Cyprus Atmospheric Observatory Nicosia station (CAO-NIC) has been made publicly available on the Zenodo repository by our co-authors. This specific subset of the study data can be accessed at https://doi.org/10.5281/zenodo.18873401 (Pikridas, Baalbaki, and Sciare, 2026).

Supplement.

Author contributions. SP, MIM, DFA, ED, MP, RB, JW, and KE contributed to the conceptualization of the study. SP, MIM, RB, NOS, KNF, SH, DG and AT performed the investigation and data curation. SP, MIM, and RB conducted the formal analysis. SP, MIM, DFA, and ED were responsible for the writing of the original draft preparation. SP, MIM, ED, MP, and RB provided the methodology. EK, MP, SH and JW handled the project administration. MIM, ED, KE, JS and DFA provided supervision. RB, MP, JW, and ED performed the validation. SP was responsible for visualization. All authors contributed to reviewing and editing the manuscript.

Competing interests. The authors declare that they have no conflict of interest.

Financial support. The PortAIR project was funded by the Irish Environmental Protection Agency (EPA) under grant number 2020-CCRP-LS.6, supported by EPA Ireland and the Department of Environment, Climate and Communications. This study has been supported financially by the RIF-EXCELLENCE/0524/0393 and H2020-EMME-CARE (GA 856612) research grant. The work has also been partially supported by European Union's Horizon Europe programme under grant agreement No 101138449 — MI-TRAP.

Review Statement.

References

Aikawa, M. and Hiraki, T.: Difference in the use of a quartz filter and a PTFE filter as first-stage filter in the four-stage filter-pack method, Water. Air. Soil Pollut., 213, 331–339, https://doi.org/10.1007/S11270-010-0388-Y/FIGURES/7, 2010.

Aldekheel, M., Farahani, V. J., and Sioutas, C.: Assessing Lifetime Cancer Risk Associated with Population Exposure to PM-Bound PAHs and Carcinogenic Metals in Three Mid- Latitude Metropolitan Cities, Toxics, 11, 697, https://doi.org/10.3390/TOXICS11080697/S1, 2023.

Amato, F., Alastuey, A., Karanasiou, A., Lucarelli, F., Nava, S., Calzolai, G., Severi, M., Becagli, S., Gianelle, V. L., Colombi, C., Alves, C., Custódio, D., Nunes, T., Cerqueira, M., Pio, C., Eleftheriadis, K., Diapouli, E., Reche, C., Minguillón, M. C., Manousakas, M. I., Maggos, T., Vratolis, S., Harrison, R. M., and Querol, X.: AIRUSE-LIFE+: A harmonized PM speciation and source apportionment in five southern European cities, Atmos. Chem. Phys., 16, 3289–3309, https://doi.org/10.5194/ACP-16-3289-2016, 2016.

Sekhar Bhowmik, H., Shukla, A., Lalchandani, V., Dave, J., Rastogi, N., Singh, V., and Nand Tripathi, S.: Inter-comparison of online and offline methods for measuring ambient heavy and trace elements 1 and water-soluble inorganic ions (NO3-, SO4 2-, NH4 + and Cl-) in PM2.5 over a heavily polluted 2 megacity, Delhi 3, n.d.

Bimenyimana, E., Pikridas, M., Oikonomou, K., Iakovides, M., Christodoulou, A., Sciare, J., and Mihalopoulos, N.: Fine aerosol sources at an urban background site in the Eastern Mediterranean (Nicosia; Cyprus): Insights from offline versus online source apportionment comparison for carbonaceous aerosols, Sci. Total Environ., 893, 164741, https://doi.org/10.1016/J.SCITOTENV.2023.164741, 2023.

Bimenyimana, E., Sciare, J., Pikridas, M., Oikonomou, K., Iakovides, M., Vasiliadou, E., Savvides, C., and Mihalopoulos, N.: Persistent high PM pollution in the Eastern Mediterranean and Middle East: Insights from long-term observations and source apportionment in Cyprus, EGUsphere, 1–23, https://doi.org/10.5194/EGUSPHERE-2025-3234, 2025.

Cadeo, L., Biffi, B., Chazeau, B., Colombi, C., Cosenza, R., Cuccia, E., Manousakas, M.-I., Daellenbach, K. R., Prévôt, A. S. H., and Vecchi, R.: Intercomparison of online and offline XRF spectrometers for determining the PM_{10} elemental composition of ambient aerosol, Atmos. Meas. Tech., 18, 6435–6448, https://doi.org/10.5194/AMT-18-6435-2025, 2025.

Caggiano, R., Sabia, S., and Speranza, A.: Trace elements and human health risks assessment of finer aerosol atmospheric particles (PM1), Environ. Sci. Pollut. Res., 26, 36423–36433, https://doi.org/10.1007/S11356-019-06756-W/TABLES/5, 2019.

CAIS-ECAC: ACTRIS Standard Procedures for In-Situ Aerosol Sampling, Measurements, and Analyses at ACTRIS Observatories, Version 1.0, Center for Aerosol In-Situ Measurement, European Center for Aerosol Calibration and Characterization, ACTRIS-ERIC, https://www.actris-ecac.eu/actris-gaw-recommendation-documents.html#Guidelines, last access: 30 March 2026, 2024.

Castaneda, C. M., Cahill, T. A., Romero, J. L., and King, R. S.: Depth profiling of hydrogen in amorphous media and applicable to quartz air filters, Nucl. Instruments Methods Phys. Res. Sect. B Beam Interact. with Mater. Atoms, 145, 553–561, https://doi.org/10.1016/S0168-583X(98)00506-0, 1998.

Chen, S.-L., Chang, S.-W., Chen, Y.-J., and Chen, H.-L.: Possible warming effect of fine particulate matter in the atmosphere, Commun. Earth Environ. 2021 21, 2, 1–9, https://doi.org/10.1038/s43247-021-00278-5, 2021.

Chiari, M., Yubero, E., Calzolai, G., Lucarelli, F., Crespo, J., Galindo, N., Nicolás, J. F., Giannoni, M., and Nava, S.: Comparison of PIXE and XRF analysis of airborne particulate matter samples collected on Teflon and quartz fibre filters, Nucl. Instruments Methods Phys. Res. Sect. B Beam Interact. with Mater. Atoms, 417, 128–132, https://doi.org/10.1016/j.nimb.2017.07.031, 2018.

Christodoulou, A., Stavroulas, I., Vrekoussis, M., Desservettaz, M., Pikridas, M., Bimenyimana, E., Kushta, J., Ivančič, M., Rigler, M., Goloub, P., Oikonomou, K., Sarda-Estève, R., Savvides, C., Afif, C., Mihalopoulos, N., Sauvage, S., and Sciare, J.: Ambient carbonaceous aerosol levels in Cyprus and the role of pollution transport from the Middle East, Atmos. Chem. Phys., 23, 6431–6456, https://doi.org/10.5194/ACP-23-6431-2023, 2023.

Diapouli, E., Manousakas, M. I., Vratolis, S., Vasilatou, V., Pateraki, S., Bairachtari, K. A., Querol, X., Amato, F., Alastuey, A., Karanasiou, A. A., Lucarelli, F., Nava, S., Calzolai, G., Gianelle, V. L., Colombi, C., Alves, C., Custódio, D., Pio, C., Spyrou, C., Kallos, G. B., and Eleftheriadis, K.: AIRUSE-LIFE +: Estimation of natural source contributions to urban ambient air PM10 and PM2. 5 concentrations in southern Europe - Implications to compliance with limit values, Atmos. Chem. Phys., 17, 3673–3685, https://doi.org/10.5194/acp-17-3673-2017, 2017.

Dinoi, A., Pavese, G., Calvello, M., Chirizzi, D., Pennetta, A., De Benedetto, G. E., Esposito, F., Mapelli, C., and Contini, D.: Characterization of aerosol and its oxidative potential in a coastal semi-rural site of Southern Italy, Atmos. Environ., 333, 120656, https://doi.org/10.1016/j.atmosenv.2024.120656, 2024.

Elvatech: ElvaX PmX-5050 Continuous Particulate Matter Monitor, https://elvatech.com/products/elvax-pmx-5050/, last access: 29 March 2026, n.d.

Fossum, K. N., Lin, C., O'Sullivan, N., Lei, L., Hellebust, S., Ceburnis, D., Afzal, A., Tremper, A., Green, D., Jain, S., Byčenkienė, S., O'Dowd, C., Wenger, J., and Ovadnevaite, J.: Two distinct ship emission profiles for organic-sulfate source apportionment of PM in sulfur emission control areas, Atmos. Chem. Phys., 24, 10815–10831, https://doi.org/10.5194/ACP-24-10815-2024, 2024.

Fossum, K., O'Sullivan, N., Jain, S., Lei, L., Lin, C., Ceburnis, D., Hellebust, S., O'Dowd, C., Ovadnevaite, J., and Wenger, J.: Source Apportionment of Air Pollution in the Dublin Port Area (PortAIR), Research 495, Environmental Protection Agency, https://www.epa.ie/publications/research/air/research-495-source-apportionment-of-air-pollution-in-the-dublin-port-area-portair.php, 2025.

Furger, M., Minguillón, M. C., Yadav, V., Slowik, J. G., Hüglin, C., Fröhlich, R., Petterson, K., Baltensperger, U., and Prévôt, A. S. H.: Elemental composition of ambient aerosols measured with high temporal resolution using an online XRF spectrometer, Atmos. Meas. Tech., 10, 2061–2076, https://doi.org/10.5194/amt-10-2061-2017, 2017.

Furger, M., Rai, P., Slowik, J. G., Cao, J., Visser, S., Baltensperger, U., and Prévôt, A. S. H.: Automated alternating sampling of PM10 and PM2.5 with an online XRF spectrometer, Atmos. Environ. X, 5, 100065, https://doi.org/10.1016/J.AEAOA.2020.100065, 2020.

Eleftheriadis, K., Gini, M. I., Diapouli, E., Vratolis, S., Vasilatou, V., Fetfatzis, P., and Manousakas, M. I.: Aerosol microphysics and chemistry reveal the COVID19 lockdown impact on urban air quality, Sci. Reports 2021 111, 11, 14477-, https://doi.org/10.1038/s41598-021-93650-6, 2021.

Gini, M., Manousakas, M., Karydas, A. G., and Eleftheriadis, K.: Mass size distributions, composition and dose estimates of particulate matter in Saharan dust outbreaks, Environ. Pollut., 298, 118768, https://doi.org/10.1016/J.ENVPOL.2021.118768, 2022.

Gupta, S., Soni, P., and Gupta, A. K.: Optimization of WD-XRF analytical technique to measure elemental abundance in PM2.5 dust collected on quartz-fibre filter, Atmos. Pollut. Res., 12, 345–351, https://doi.org/10.1016/j.apr.2021.01.001, 2021.

Healy, R. M., O'Connor, I. P., Hellebust, S., Allanic, A., Sodeau, J. R., and Wenger, J. C.: Characterisation of single particles from in-port ship emissions, Atmos. Environ., 43, 6408–6414, https://doi.org/10.1016/J.ATMOSENV.2009.07.039, 2009.

Hopke, P. K., Dai, Q., Li, L., and Feng, Y.: Global review of recent source apportionments for airborne particulate matter, Sci. Total Environ., 740, 140091, https://doi.org/10.1016/J.SCITOTENV.2020.140091, 2020.

HORIBA: PX-375 Continuous Particulate Monitor with X-ray Fluorescence, https://www.horiba.com/int/process-and-environmental/products/detail/action/show/Product/px-375-181/, last access: 29 March 2026, n.d.

Huang, R. J., Cheng, R., Jing, M., Yang, L., Li, Y., Chen, Q., Chen, Y., Yan, J., Lin, C., Wu, Y., Zhang, R., El Haddad, I., Prevot, A. S. H., O'Dowd, C. D., and Cao, J.: Source-Specific Health Risk Analysis on Particulate Trace Elements: Coal Combustion and Traffic Emission As Major Contributors in Wintertime Beijing, Environ. Sci. Technol., 52, 10967–10974, https://doi.org/10.1021/ACS.EST.8B02091/ASSET/IMAGES/LARGE/ES-2018-02091R_0004.JPEG, 2018.

Jain, S., Sharma, S. K., Vijayan, N., and Mandal, T. K.: Seasonal characteristics of aerosols (PM2.5 and PM10) and their source apportionment using PMF: A four year study over Delhi, India, Environ. Pollut., 262, 114337, https://doi.org/10.1016/j.envpol.2020.114337, 2020.

Jang, H. N., Seo, Y. C., Lee, J. H., Hwang, K. W., Yoo, J. I., Sok, C. H., and Kim, S. H.: Formation of fine particles enriched by V and Ni from heavy oil combustion: Anthropogenic sources and drop-tube furnace experiments, Atmos. Environ., 41, 1053–1063, https://doi.org/10.1016/J.ATMOSENV.2006.09.011, 2007.

Khuzestani, R. B., Schauer, J. J., Wei, Y., Zhang, Y., and Zhang, Y.: A non-destructive optical color space sensing system to quantify elemental and organic carbon in atmospheric particulate matter on Teflon and quartz filters, Atmos. Environ., 149, 84–94, https://doi.org/10.1016/J.ATMOSENV.2016.11.002, 2017.

Manousakas, M., Diapouli, E., Papaefthymiou, H., Kantarelou, V., Zarkadas, C., Kalogridis, A.-C., Karydas, A.-G., and Eleftheriadis, K.: XRF characterization and source apportionment of PM10 samples collected in a coastal city, X-Ray Spectrom., 47, 190–200, https://doi.org/10.1002/xrs.2817, 2018.

Manousakas, M., Diapouli, E., Belis, C., Vasilatou, V., Gini, M., Lucarelli, F., Querol, X., and Eleftheriadis, K.: Quantitative assessment of the variability in chemical profiles from source apportionment analysis of PM10 and PM2.5 at different sites within a large metropolitan area, Environ. Res., 192, 110257, https://doi.org/10.1016/J.ENVRES.2020.110257, 2021.

Manousakas, M., Furger, M., Daellenbach, K. R., Canonaco, F., Chen, G., Tobler, A., Rai, P., Qi, L., Tremper, A. H., Green, D., Hueglin, C., Slowik, J. G., El Haddad, I., and Prevot, A. S. H.: Source identification of the elemental fraction of particulate matter using size segregated, highly time-resolved data and an optimized source apportionment approach, Atmos. Environ. X, 14, 100165, https://doi.org/10.1016/J.AEAOA.2022.100165, 2022.

Megido, L., Suárez-Peña, B., Negral, L., Castrillón, L., and Fernández-Nava, Y.: Suburban air quality: Human health hazard assessment of potentially toxic elements in PM10, Chemosphere, 177, 284–291, https://doi.org/10.1016/J.CHEMOSPHERE.2017.03.009, 2017.

Ostro, B., Tobias, A., Karanasiou, A., Samoli, E., Querol, X., Rodopoulou, S., Basagaña, X., Eleftheriadis, K., Diapouli, E., Vratolis, S., Jacquemin, B., Katsouyanni, K., Sunyer, J., Forastiere, F., Stafoggia, M., Alessandrini, E., Angelini, P., Berti, G., Bisanti, L., Cadum, E., Catrambone, M., Chiusolo, M., Davoli, M., De'Donato, F., Demaria, M., Gandini, M., Grosa, M., Faustini, A., Ferrari, S., F, F., Pandolfi, P., Pelosini, R., Perrino, C., Pietrodangelo, A., Pizzi, L., Poluzzi, V., Randi, G., Ranzi, A., Rowinski, M., Scarinzi, C., S, M., Stivanello, E., ZauliSajani, S., Dimakopoulou, K., E, K., K, K., Kelessis, A. G., Maggos, T., Mihalopoulos, N., Pateraki, S., Petrakakis, M., R, S., S, E., Sypsa, V., Agis, D., Artiñano, B., BarreraGómez, J., B, X., De La Rosa, J., Diaz, J., Fernandez, R., J, B., K, A., Linares, C., O, B., Perez, N., Pey, J., Q, X., Sanchez, A. M., S, J., T, A., Bidondo, M., Declercq, C., Le Tertre, A., Lozano, P., Medina, S., Pascal, L., and Pascal, M.: The risks of acute exposure to black carbon in Southern Europe: results from the MED-PARTICLES project, Occup. Environ. Med., 72, 123–129, https://doi.org/10.1136/OEMED-2014-102184, 2015.

Pikridas, M., Baalbaki, R., and Sciare, J.: Dataset for: Near Real-Time & Benchtop XRF Intercomparison for PM Elemental Analysis on Quartz and Teflon Filters: A Case Study Across Three European Cities — Cyprus Atmospheric Observatory Nicosia Station (CAO-NIC) Data, Zenodo [data set], https://doi.org/10.5281/zenodo.18873401, 2026.

Potì, S., Merico, E., Conte, M., Unga, F., Cesari, D., Dinoi, A., De Bartolomeo, A. R., Pennetta, A., Bloise, E., Deluca, G., De Benedetto, G. E., Ferrera, R., Bompadre, E., Guascito, M. R., and Contini, D.: Spatial and seasonal variability of the contribution of sources to PM2.5, PM10 and their oxidative potential in different sites in a central Mediterranean area, Sci. Total Environ., 976, 179283, https://doi.org/10.1016/j.scitotenv.2025.179283, 2025.

Rai, P.: Analysis of major and trace elements in ambient aerosols and their sources in European and Asian cities, PhD thesis, ETH Zurich, https://doi.org/10.3929/ethz-b-000440336, 2020.

Rai, P., Furger, M., Slowik, J. G., Canonaco, F., Fröhlich, R., Hüglin, C., Minguillón, M. C., Petterson, K., Baltensperger, U., and Prévôt, A. S. H.: Source apportionment of highly time-resolved elements during a firework episode from a rural freeway site in Switzerland, Atmos. Chem. Phys., 20, 1657–1674, https://doi.org/10.5194/acp-20-1657-2020, 2020.

Rhodes, E. P., Ren, Z., and Mays, D. C.: Zinc leaching from tire crumb rubber, Environ. Sci. Technol., 46, 12856–12863, https://doi.org/10.1021/ES3024379/SUPPL_FILE/ES3024379_SI_001.PDF, 2012.

Samoli, E., Stafoggia, M., Rodopoulou, S., Ostro, B., Declercq, C., Alessandrini, E., Díaz, J., Karanasiou, A., Kelessis, A. G., Tertre, A. Le, Pandolfi, P., Randi, G., Scarinzi, C., Zauli-Sajani, S., Katsouyanni, K., Forastiere, F., Alessandrini, E., Angelini, P., Berti, G., Bisanti, L., Cadum, E., Catrambone, M., Chiusolo, M., Davoli, M., de' Donato, F., Demaria, M., Gandini, M., Grosa, M., Faustini, A., Ferrari, S., Forastiere, F., Pandolfi, P., Pelosini, R., Perrino, C., Pietrodangelo, A., Pizzi, L., Poluzzi, V., Priod, G., Randi, G., Ranzi, A., Rowinski, M., Scarinzi, C., Stivanello, E., Zauli-Sajani, S., Dimakopoulou, K., Elefteriadis, K., Katsouyanni, K., G.Kelessis, A., Maggos, T., Michalopoulos, N., Pateraki, S., Petrakakis, M., Rodopoulou, S., Samoli, E., Sypsa, V., Agis, D., Alguacil, J., Artiñano, B., Barrera-Gómez, J., Basagaña, X., de la Rosa, J., Diaz, J., Fernandez, R., Jacquemin, B., Linares, C., Ostro, B., Pérez, N., Pey, J., Querol, X., Sanchez, A., Sunyer, J., Tobias, A., Bidondo, M., Declercq, C., Le Tertre, A., Lozano, P., Medina, S., Pascal, L., and Pascal, M.: Associations between fine and coarse particles and mortality in Mediterranean cities: Results from the MED-PARTICLES project, Environ. Health Perspect., 121, 932–938, https://doi.org/10.1289/EHP.1206124, 2013.

SailBri Cooper Inc.: Xact 625i Ambient Continuous Multi-Metals Monitor, https://sci-monitoring.com/product/xact-625i-ambient-continuous-multi-metals-monitor/, last access: 29 March 2026, n.d.

Schoonjans, T., Solé, V. A., Vincze, L., Sanchez Del Rio, M., Appel, K., and Ferrero, C.: A general Monte Carlo simulation of energy-dispersive X-ray fluorescence spectrometers - Part 6. Quantification through iterative simulations, Spectrochim. Acta - Part B At. Spectrosc., 82, 36–41, https://doi.org/10.1016/j.sab.2012.12.011, 2013.

Skalny, A. V., Lima, T. R. R., Ke, T., Zhou, J. C., Bornhorst, J., Alekseenko, S. I., Aaseth, J., Anesti, O., Sarigiannis, D. A., Tsatsakis, A., Aschner, M., and Tinkov, A. A.: Toxic metal exposure as a possible risk factor for COVID-19 and other respiratory infectious diseases, Food Chem. Toxicol., 146, 111809, https://doi.org/10.1016/J.FCT.2020.111809, 2020.

Suárez-Peña, B., Negral, L., Castrillón, L., Megido, L., Marañón, E., and Fernández-Nava, Y.: Imaging Techniques and Scanning Electron Microscopy as Tools for Characterizing a Si-Based Material Used in Air Monitoring Applications, Mater. 2016, Vol. 9, Page 109, 9, 109, https://doi.org/10.3390/MA9020109, 2016.

Thorpe, A. and Harrison, R. M.: Sources and properties of non-exhaust particulate matter from road traffic: A review, Sci. Total Environ., 400, 270–282, https://doi.org/10.1016/J.SCITOTENV.2008.06.007, 2008.

Tremper, A. H., Font, A., Priestman, M., Hamad, S. H., Chung, T.-C., Pribadi, A., Brown, R. J. C., Goddard, S. L., Grassineau, N., Petterson, K., Kelly, F. J., and Green, D. C.: Field and laboratory evaluation of a high time resolution x-ray fluorescence instrument for determining the elemental composition of ambient aerosols, Atmos. Meas. Tech., 11, 3541–3557, https://doi.org/10.5194/amt-11-3541-2018, 2018.

Unga, F., Calzolai, G., Chiari, M., Cuccia, E., Colombi, C., Franciosa, M., Dinoi, A., Merico, E., Pennetta, A., Gómez-Sánchez, N., Mapelli, C., Pareti, S., Perrino, C., Yubero, E., and Contini, D.: Determination of aerosol composition by ED-XRF on Teflon and quartz substrates: potentialities and limits, Aerosol Res, 3, 405–415, https://doi.org/10.5194/ar-3-405-2025, 2025.

Vecchi, R., Valli, G., Fermo, P., D'Alessandro, A., Piazzalunga, A., and Bernardoni, V.: Organic and inorganic sampling artefacts assessment, Atmos. Environ., 43, 1713–1720, https://doi.org/10.1016/J.ATMOSENV.2008.12.016, 2009.

Viana, M., Kuhlbusch, T. A. J., Querol, X., Alastuey, A., Harrison, R. M., Hopke, P. K., Winiwarter, W., Vallius, M., Szidat, S., Prévôt, A. S. H., Hueglin, C., Bloemen, H., Wåhlin, P., Vecchi, R., Miranda, A. I., Kasper-Giebl, A., Maenhaut, W., and Hitzenberger, R.: Source apportionment of particulate matter in Europe: A review of methods and results, https://doi.org/10.1016/j.jaerosci.2008.05.007, 1 October 2008.

Windell, L. C., Mbengue, S., Pokorná, P., Schwarz, J., Prévôt, A. S. H., Manousakas, M. I., Papagiannis, S., Ondráček, J., Prokeš, R., and Ždímal, V.: Xact625i vs. PX-375: a comparative study of online XRF ambient multi-metal monitors vs. ICP-MS, Atmos. Meas. Tech., 18, 7021–7038, https://doi.org/10.5194/AMT-18-7021-2025, 2025.

Yatkin, S., Gerboles, M., and Borowiak, A.: Evaluation of standardless EDXRF analysis for the determination of elements on PM10 loaded filters, Atmos. Environ., 54, 568–582, https://doi.org/10.1016/J.ATMOSENV.2012.02.062, 2012.

Žitnik, M., Pelicon, P., Grlj, N., Karydas, A. G., Sokaras, D., Schütz, R., and Kanngießer, B.: Three-dimensional imaging of aerosol particles with scanning proton microprobe in a confocal arrangement, Appl. Phys. Lett., 93, 94104, https://doi.org/10.1063/1.2976163/764942, 2008.

Zografou, O., Gini, M., Manousakas, M. I., Chen, G., Kalogridis, A. C., Diapouli, E., Pappa, A., and Eleftheriadis, K.: Combined organic and inorganic source apportionment on yearlong ToF-ACSM dataset at a suburban station in Athens, Atmos. Meas. Tech., 15, 4675–4692, https://doi.org/10.5194/AMT-15-4675-2022, 2022.